



# Target detection using weather radars and electromagnetic vector sensors<sup>☆</sup>



G.V. Prateek<sup>a</sup>, Martin Hurtado<sup>b</sup>, Arye Nehorai<sup>a,\*</sup>

<sup>a</sup>Preston M. Green Department of Electrical and Systems Engineering, Washington University in St. Louis, St. Louis, MO 63130, USA

<sup>b</sup>Department of Electrical Engineering, National University of La Plata, La Plata 1900, Argentina

## ARTICLE INFO

### Article history:

Received 21 September 2016

Revised 13 February 2017

Accepted 15 February 2017

Available online 17 February 2017

### Keywords:

Target detection

Electromagnetic vector sensors

Passive radar

Weather radar

## ABSTRACT

We propose a method to detect a target in a bistatic passive polarimetric radar network, with weather surveillance radar as our illuminator of opportunity (IO). We build our signal model using electromagnetic vector sensors (EMVS) as the receiver, which captures the reflections from a point-like target present in the scene of interest, surrounded with strong clutter. We develop a generalized likelihood ratio test (GLRT) detector that is robust to inhomogeneous clutter. We also develop a maximum likelihood (ML) solution to extract the signal subspace from the received data contaminated by the clutter interference. We provide the exact distribution of the test statistic for the asymptotic case and evaluate its performance loss by considering a reduced set of data. The proposed GLRT method is a constant false alarm rate (CFAR) detector, which makes it robust against the inhomogeneous clutter. With the help of numerical results, we demonstrate the robustness and the limitations of our proposed method.

© 2017 Elsevier B.V. All rights reserved.

## 1. Introduction

Improving the detection performance of a target can be important for military and surveillance operations. Over the last decade, there has been a growing interest in the radar research community to use available signals such as, FM radio waves, television and audio broadcast signals, and satellite and mobile communication based signals, as illuminators of opportunity (IO), with one or several receivers, co-located or distributed randomly, measuring the echoes generated from the target of interest [1–3]. In general, a radar network consisting of non-cooperative IOs and one or several passive receivers is referred to as a passive radar network. Because the network uses available signals of opportunity, the need to build sophisticated infrastructure for the transmitter is avoided, thereby reducing the overall cost of the network. In addition, the receivers are smaller, cheaper, consume less power, and can be easily deployed, making the network less vulnerable to electronic counter measures and better able to counter stealth technology [4]. In this paper, we propose a passive bistatic network, with weather surveillance radar as the IO and electromag-

netic vector sensor (EMVS) [5] as the receiver. To the best of our knowledge, no previous work on passive bistatic radar addressed employing a weather radar for target detection.

The signal arriving at the receiver consists of the signal from the non-cooperative transmitter (transmitter-to-receiver), which is referred to as the reference channel, and the echoes generated by the reflection of the transmitted signal from the target (target-to-receiver), which are referred to as the surveillance channel. Conventionally, spatial and temporal filtering techniques isolate the reference from the surveillance channel. For target detection, the transmitted signal is estimated from the reference channel, and cross-correlated with the signal in the surveillance channel. The resulting function called the cross-ambiguity function (CAF) [6–9], mimics a matched filter output. The performance of the CAF-based detector degrades depending on the signal strengths of the surveillance and reference channel. In some scenarios, the direct path signal that is received via the side lobes of the receiver antenna is likely to mask the target echoes. In such cases, the Doppler and delay are estimated either by cancellation of the direct path [10] or applying the modified cross-correlation method [11]. On the other hand, when a good estimate of the reference channel signal is not available, which occurs due to propagation losses, and blockage or non-availability of the line-of-sight, only the surveillance channel is considered for target detection.

A generalized likelihood ratio test (GLRT) represents a solution to the passive radar detection problem when a good estimate of

<sup>☆</sup> This work was supported by the AFOSR Grants FA9550-11-1-0210 and FA9550-16-1-0386.

\* Corresponding author.

E-mail addresses: [prateek@ese.wustl.edu](mailto:prateek@ese.wustl.edu) (G.V. Prateek),

[martin.hurtado@ing.unlp.edu.ar](mailto:martin.hurtado@ing.unlp.edu.ar) (M. Hurtado), [nehorai@ese.wustl.edu](mailto:nehorai@ese.wustl.edu) (A. Nehorai).

the transmitted signal is not available in the reference channel. Only the surveillance channel is considered, due to which the detector does not require knowledge of reference channel signal-to-noise ratio (SNR). Hack et al. [12] present a GLRT-based detector in a passive network of non-overlapping frequency band. A similar approach is presented in [13,14] for a multistatic passive radar network. Building on a GLRT framework, Wang and Yazici [15] describe a passive imaging detector based on electromagnetic signal modeling.

There are 150 nearly identical dual-polarized S-band Doppler weather surveillance radars in the USA, with an observation range of 230–460 km and a range resolution of 0.25–1 km, depending on the mode of operation [16]. The radar operates according to selected scanning pattern using high-power transmitter and mechanically-rotated antenna, with a minimum and maximum elevation angle of 0.5° and 20°, respectively. Due to the high elevation angle and its corresponding volume coverage pattern (VCP), along with the rotating platform of the transmitter, minimal direct-path signal is observed by the receiver located on the ground in the reference channel. However, because of the high sensitivity of a weather radar [17], the received echoes contain reflections from clouds and precipitation in addition to the signal of interest. In such scenarios, the signal models presented in [12,14] cannot be applied. In general, the target is anisotropic in nature whose scattering parameters are unknown. To overcome these problems, we develop a polarimetric signal model that considers the effect of inhomogeneous clutter and noise at the receiver. We make realistic assumptions in our signal model, where the clutter reflections are generated from an unknown covariance matrix depending on the hydrometeors present in the range gate of interest [18, Chapter 7]. We believe we are the first to consider polarization information for mitigating signal-dependent clutter and improve detection in a passive radar, with weather surveillance radar as IO. The goal of this paper is to detect a target, using a passive bistatic radar network of electromagnetic vector sensors and a weather surveillance radar as the illuminator of opportunity, in the presence of signal-dependent clutter.

The remainder of this paper is organized as follows. Signal, clutter, and noise models are explained in detail in Section 2. In Sections 3.1–3.3, we derive a detector based on the GLRT framework and provide a closed form expression of the distribution of the test statistic in Section 3.4. The expression of the probability of false alarm does not depend on the transmitted signal, clutter, and receiver noise, which indicates the proposed GLRT method is a constant false alarm rate (CFAR) detector. In Section 4, we analyze the performance of the proposed detector through numerical simulations. We vary the system settings, such as the number of snapshots, and the clutter-to-noise ratio (CNR), and we determine the performance of the detector by plotting the curves for the probability of detection. Finally, the paper is summarized in Section 5.

**Notations:** Bold uppercase and calligraphic uppercase letters denote matrices. Bold lowercase letters denote vectors. Scalars are denoted by both lowercase and uppercase letters. For any complex matrix  $\mathbf{A}$ , we use  $\mathbf{A}^T$ ,  $\mathbf{A}^H$ ,  $\mathbf{A}^*$ ,  $\mathbf{A}^{-1}$ ,  $\mathbf{A}^\dagger$ ,  $\text{Tr}\{\mathbf{A}\}$ , and  $|\mathbf{A}|$  to denote the transpose, conjugate-transpose, conjugate, inverse, pseudo-inverse, trace, and determinant of  $\mathbf{A}$ , respectively. Additionally,  $\mathbf{I}_N$  represent identity of dimension  $N$ . The matrices  $\mathbf{P}_A$  and  $\mathbf{P}_A^\perp$  denotes projection matrix of  $\mathbf{A}$  and its orthogonal projection matrix, respectively.  $\otimes$  stands for the Kronecker product,  $\rightarrow$  denotes convergence, and  $\|\cdot\|$  represents the  $\ell_2$ -norm. Further,  $j$  represents  $\sqrt{-1}$ ,  $\mathcal{CN}$  stands for complex normal distribution,  $\Re$  and  $\Im$  denote the real-part and imaginary-part of a complex number, respectively, and  $\mathbb{E}[\cdot]$  represents the expectation operator.

## 2. Signal model and statistics

### 2.1. Signal model

We consider a dual-polarized weather radar located at  $\mathbf{t} = [t_x, t_y, t_z]^T \in \mathbb{R}^3$  as the illuminator of opportunity in our signal model. The polarimetric representation of the transmitted complex bandpass signal is given by  $\mathbf{Q}_\alpha \mathbf{w}_\beta s(t) e^{j\Omega_c t}$  where

$$\mathbf{Q}_\alpha = \begin{bmatrix} \cos \alpha & \sin \alpha \\ -\sin \alpha & \cos \alpha \end{bmatrix}, \quad \mathbf{w}_\beta = \begin{bmatrix} \cos \beta \\ j \sin \beta \end{bmatrix}, \quad (1)$$

$\alpha$  and  $\beta$  represent the orientation and ellipticity of polarization of the transmitted signal, respectively, and  $\Omega_c$  is the carrier frequency. The signal  $s(t)$  is the complex baseband signal,  $t \in [0, T]$ , where  $T/2$  is the pulse repetition interval (PRI) of a dual-polarized transmitter, which sends sequentially two pulses of orthogonal polarization. Exploiting the polarimetric information provides useful information about the target, such as its geometry, material, and orientation. In order to capture this polarimetric information, we need to use diversely polarized antennas. One popular category of such antennas includes the electromagnetic vector sensors [5], where the electric dipoles and electric loops are aligned within the three axes of the coordinate system. Let  $(\theta, \phi)$  denote the azimuth and elevation angle, respectively, of a hypothesized target located at  $\mathbf{p} = [p_x, p_y, p_z]^T \in \mathbb{R}^3$  and traveling with a velocity  $\dot{\mathbf{p}} = [\dot{p}_x, \dot{p}_y, \dot{p}_z]^T \in \mathbb{R}^3$ , as seen by the receiver. The steering matrix of an electromagnetic vector sensor denoted as  $\mathbf{D}_{\theta, \phi} \in \mathbb{R}^{6 \times 2}$  can be parameterized as [5]

$$\mathbf{D}_{\theta, \phi} = \begin{bmatrix} -\sin \theta & -\cos \theta \sin \phi \\ \cos \theta & -\sin \theta \sin \phi \\ 0 & \cos \phi \\ -\cos \theta \sin \phi & \sin \phi \\ -\sin \theta \sin \phi & -\cos \phi \\ \cos \phi & 0 \end{bmatrix}. \quad (2)$$

Special cases of the steering matrix in (2) are the tripole antenna [19] and the classical polarization radar using vertical and horizontal linear polarization. The target and the background clutter are characterized by their scattering matrices, which depend on the angle of view and the frequency of the transmitted signal. Let  $\mathbf{S}_p \in \mathbb{C}^{2 \times 2}$  and  $\mathbf{S}_c \in \mathbb{C}^{2 \times 2}$  denote the hypothesized target and clutter scattering matrix coefficients, respectively, as seen by the receiver located at coordinates  $\mathbf{r} = [r_x, r_y, r_z]^T \in \mathbb{R}^3$ , where  $\mathbf{S}_p$  and  $\mathbf{S}_c$  are parameterized as [20]

$$\mathbf{S}_p = \begin{bmatrix} \sigma_p^{hh} & \sigma_p^{hv} \\ \sigma_p^{vh} & \sigma_p^{vv} \end{bmatrix} \quad \text{and} \quad \mathbf{S}_c = \begin{bmatrix} \sigma_c^{hh} & \sigma_c^{hv} \\ \sigma_c^{vh} & \sigma_c^{vv} \end{bmatrix}. \quad (3)$$

The coefficients  $\sigma_{(p,c)}^{hh}$  and  $\sigma_{(p,c)}^{vv}$  represent the co-polar scattering coefficients, and the variables  $\sigma_{(p,c)}^{vh}$  and  $\sigma_{(p,c)}^{hv}$  represent the cross-polar scattering coefficients. The complex envelope at the output of the quadrature receiver can be expressed as

$$\mathbf{y}(t) = \mathbf{D}_{\theta, \phi} \mathbf{S}_p \mathbf{Q}_\alpha \mathbf{w}_\beta s(t - \tau_p) e^{j\Omega_D t} e^{-j\Omega_c \tau_p} + \mathbf{D}_{\theta, \phi} \mathbf{S}_c \mathbf{Q}_\alpha \mathbf{w}_\beta s(t - \tau_c) e^{-j\Omega_c \tau_c} + \mathbf{e}(t), \quad (4)$$

where

$$\Omega_D = \frac{\Omega_c}{c} \left[ \frac{(\mathbf{r} - \mathbf{p})^T \dot{\mathbf{p}}}{\|\mathbf{r} - \mathbf{p}\|} + \frac{(\mathbf{p} - \mathbf{t})^T \dot{\mathbf{p}}}{\|\mathbf{p} - \mathbf{t}\|} \right],$$

and  $\tau_p = \frac{\|\mathbf{r} - \mathbf{p}\| + \|\mathbf{p} - \mathbf{t}\|}{c}$ . (5)

Here,  $\tau_p$  represents the time it takes for the signal to travel from the transmitter to the target, and from the target to the receiver.  $\Omega_D$  represents the Doppler shift in the signal,  $c$  is the speed of the

propagation of the electromagnetic wave, and  $\mathbf{e}(t)$  is the complex baseband thermal noise. The Doppler frequency shift in (5) is computed based on the relative motion between the transmitter and the target, and the target and receiver in a passive bistatic radar geometry [21]. In Eq. (4), we assume that the target moves with a certain velocity,  $\dot{\mathbf{p}}$ , and the Doppler frequency shift produced by the clutter is zero. The signal model in (4) can be easily extended to a known non-zero Doppler frequency shift produced by the clutter. Since the weather radar operates at high elevation angles, the type of clutter we are dealing with in our signal model is a meteorological hydrometeor. Also, it is reasonable to assume that the receiver has a good prior knowledge of the Doppler frequency shift produced by clutter through Level II and Level III weather radar data products, which are available for commercial applications and updated regularly. Further, we assume that  $\tau_c$  is known and is approximately equal to the time it takes for the transmitted signal to travel from the transmitter to the center of the range cell, and from the center of the range cell to the receiver. Based on this assumption,  $\tau_p = \tau_c + \Delta\tau_p$ , where  $\Delta\tau_p$  accounts for the shift in the target's position from the center of the range cell. Compensating for the absolute phase term  $e^{-j\Omega_c\tau_c}$ , the received signal in (4) can be written as

$$\mathbf{y}(t) = \mathbf{D}_{\theta,\phi} \mathbf{S}_p \mathbf{Q}_\alpha \mathbf{w}_\beta s(t - \tau_p) e^{j\Omega_D t} e^{-j\Omega_c \Delta\tau_p} + \mathbf{D}_{\theta,\phi} \mathbf{S}_c \mathbf{Q}_\alpha \mathbf{w}_\beta s(t - \tau_c) + \mathbf{e}(t). \quad (6)$$

We introduce the vectorized scattering matrix coefficients,  $\mathbf{x}_p = e^{-j\Omega_c \Delta\tau_p} [\sigma_p^{hh}, \sigma_p^{vv}, \sigma_p^{hv}, \sigma_p^{vh}]^T$  and  $\mathbf{x}_c = [\sigma_c^{hh}, \sigma_c^{vv}, \sigma_c^{hv}, \sigma_c^{vh}]^T$ , that denote the target and clutter reflectivity coefficients, respectively. Let  $\boldsymbol{\epsilon}_{\alpha,\beta} \triangleq [\epsilon_1, \epsilon_2]^T = \mathbf{Q}_\alpha \mathbf{w}_\beta$  denote the polarization vector. We define polarization matrix as [22]

$$\bar{\boldsymbol{\epsilon}}_{\alpha,\beta} = \begin{bmatrix} \epsilon_1 & 0 & \epsilon_2 & 0 \\ 0 & \epsilon_2 & 0 & \epsilon_1 \end{bmatrix}. \quad (7)$$

where  $\text{rank}(\bar{\boldsymbol{\epsilon}}_{\alpha,\beta}) = 2$ . Then, the received signal in (6) can be rewritten as

$$\mathbf{y}(t) = \mathbf{D}_{\theta,\phi} \bar{\boldsymbol{\epsilon}}_{\alpha,\beta} \mathbf{x}_p s(t - \tau_p) e^{j\Omega_D t} + \mathbf{D}_{\theta,\phi} \bar{\boldsymbol{\epsilon}}_{\alpha,\beta} \mathbf{x}_c s(t - \tau_c) + \mathbf{e}(t). \quad (8)$$

We define a snapshot as a signal that contains both orthogonal polarized waveforms of the transmitted signal. The received signal is sampled at every  $\Delta t$  seconds, where  $\Delta t$  represents the fast-time sampling interval. Let the number of samples in each range gate be  $N$ , where  $N$  is even. We define  $s[n]$  of a continuous-time signal  $s(t)$  as  $s[n] = s(n\Delta t)$ . We denote the time delay and Doppler shift in the sampled signal domain as  $n_p = \tau_p/\Delta t$ ,  $n_c = \tau_c/\Delta t$ , and  $\omega_D = \Omega_D \Delta t$ , respectively. After sampling, the signal received by the EMVS at time  $n\Delta t$  becomes

$$\mathbf{y}[n] = \mathbf{D}_{\theta,\phi} \bar{\boldsymbol{\epsilon}}_{\alpha,\beta} \mathbf{x}_p s[n - n_p] e^{j\omega_D n} + \mathbf{D}_{\theta,\phi} \bar{\boldsymbol{\epsilon}}_{\alpha,\beta} \mathbf{x}_c s[n - n_c] + \mathbf{e}[n]. \quad (9)$$

If the time samples are stacked in a vector, (9) can be written as

$$\mathbf{y} = (\mathbf{s}(n_p, \omega_D) \otimes \mathbf{D}_{\theta,\phi} \bar{\boldsymbol{\epsilon}}_{\alpha,\beta}) \mathbf{x}_p + (\mathbf{s}(n_c, 0) \otimes \mathbf{D}_{\theta,\phi} \bar{\boldsymbol{\epsilon}}_{\alpha,\beta}) \mathbf{x}_c + \mathbf{e} \quad (10)$$

where

$$\mathbf{y} = [\mathbf{y}[0]^T, \mathbf{y}[1]^T, \dots, \mathbf{y}[N-1]^T]^T,$$

$$\mathbf{s}(n_p, \omega_D) = [s(-n_p) e^{j(0)\omega_D}, \dots, s(N-1-n_p) e^{j(N-1)\omega_D}]^T,$$

$$\mathbf{s}(n_c, 0) = [s(-n_c), \dots, s(N-1-n_c)]^T,$$

$$\mathbf{e} = [\mathbf{e}[0]^T, \mathbf{e}[1]^T, \dots, \mathbf{e}[N-1]^T]^T.$$

Let  $\mathbf{F}_N \in \mathbb{C}^{N \times N}$  denote the unitary discrete Fourier transform (DFT) matrix such that the  $(m, n)^{\text{th}}$  element is

$$[\mathbf{F}]_{m,n} = \frac{1}{\sqrt{N}} e^{-j\frac{2\pi}{N} mn}$$

for  $m, n = 0, \dots, N-1$ . Let  $\mathbf{L}_N(x) \in \mathbb{C}^{N \times N}$  denote a diagonal matrix such that

$$\mathbf{L}_N(x) = \text{diag} \{ e^{j(0)x}, e^{j(1)x}, \dots, e^{j(N-1)x} \}$$

where  $\text{diag}\{\cdot\}$  represents a diagonal matrix. Then, the received signal in (10) can be represented as [12]

$$\mathbf{y} = (\mathcal{D}_{n_p, \omega_D} \mathbf{s} \otimes \mathbf{D}_{\theta,\phi} \bar{\boldsymbol{\epsilon}}_{\alpha,\beta}) \mathbf{x}_p + (\mathcal{D}_{n_c, 0} \mathbf{s} \otimes \mathbf{D}_{\theta,\phi} \bar{\boldsymbol{\epsilon}}_{\alpha,\beta}) \mathbf{x}_c + \mathbf{e} \quad (11)$$

where

$$\mathcal{D}_{n, \omega} = \mathbf{L}_N(\omega) \mathbf{F}_N^H \mathbf{L}_N(-2\pi n/N) \mathbf{F}_N$$

is the delay-Doppler matrix and  $\mathbf{s} = [s(0), \dots, s(N-1)]^T$ . The delay-Doppler matrix is unitary, i.e.,  $\mathcal{D}_{n, \omega}^H \mathcal{D}_{n, \omega} = \mathbf{I}_N$ . Using Kronecker product property in [23], we rewrite (11) as

$$\mathbf{y} = (\mathcal{D}_{n_p, \omega_D} \otimes \mathbf{D}_{\theta,\phi}) (\mathbf{s} \otimes \bar{\boldsymbol{\epsilon}}_{\alpha,\beta}) \mathbf{x}_p + (\mathcal{D}_{n_c, 0} \otimes \mathbf{D}_{\theta,\phi}) (\mathbf{s} \otimes \bar{\boldsymbol{\epsilon}}_{\alpha,\beta}) \mathbf{x}_c + \mathbf{e}. \quad (12)$$

For notation simplicity, we denote  $\mathbf{A} = \mathcal{D}_{n_c, 0} \otimes \mathbf{D}_{\theta,\phi} \in \mathbb{C}^{L \times M}$ ,  $\mathbf{B} = \mathcal{D}_{n_p, \omega_D} \otimes \mathbf{D}_{\theta,\phi} \in \mathbb{C}^{L \times M}$ , and  $\mathbf{S} = \mathbf{s} \otimes \bar{\boldsymbol{\epsilon}}_{\alpha,\beta} \in \mathbb{C}^{M \times P}$ , where we drop the dependency on delay, Doppler, direction of arrival, orientation, and ellipticity. Note that  $\mathbf{A}$  and  $\mathbf{B}$  are analogous to a steering matrix in (2) with delay-Doppler information embedded in them. In addition, the dimensions of  $\mathbf{A}$  and  $\mathbf{B}$  depends on the type of the receiver antenna, and the inner product  $\mathbf{A}^H \mathbf{A} = \mathbf{B}^H \mathbf{B} = k \mathbf{I}_M$ . For an EMVS receiver<sup>1</sup>,  $L = 6N$ ,  $M = 2N$ ,  $P = 4$ , and  $k = 2$ . Based on the simplified notation (12) can be written as

$$\mathbf{y} = \mathbf{B} \mathbf{S} \mathbf{x}_p + \mathbf{A} \mathbf{S} \mathbf{x}_c + \mathbf{e}. \quad (13)$$

In Eq. (13), the  $\text{rank}(\mathbf{S}) = P$ , i.e., the signal matrix that contains information about the waveform and polarization of the transmitted signal, is full-rank. By the definition of a snapshot in our signal model, we consider two orthogonal polarized waveforms. For example, in the case of orthogonal polarization, the first  $N/2$  samples are transmitted with  $\beta = 0$  and  $\alpha = -\pi/4$ , and the next  $N/2$  samples are transmitted with  $\beta = 0$  and  $\alpha = \pi/4$ . Weather surveillance radars (WSR-88D) employ alternating transmission of horizontal and vertical polarized waveforms [24]. Due to the orthogonal polarization of the transmitted signal, the signal information matrix attains full-rank. Further, Hochwald and Nehorai [25, Eq. (6.3)] show that the inner product of the signal information matrix for orthogonal polarized waveforms reduces to the form of a scalar times the identity matrix, where the scalar value depends on the energy of the transmitted waveform. For simplicity, we assume that the transmitted signal is unit energy, which reduces the inner product of the signal information matrix to an identity matrix.

## 2.2. Signal, clutter, and noise statistics

The non-cooperative nature of the transmitter makes the signal information matrix,  $\mathbf{S}$ , deterministic and *unknown*. The receiver noise vector,  $\mathbf{e}$ , is a zero mean complex Gaussian random vector with covariance  $\sigma \mathbf{I}_L$ , where we assume  $\sigma$  is *known*. In other words, the noise measurements are independent across different samples but have the same power. We consider clutter to consist of many point-like scatters producing incoherent reflections around the range cell. Because these reflections are random, the aggregate scattering coefficients of the clutter,  $\mathbf{x}_c$ , are assumed to be distributed as zero mean complex Gaussian random vectors with *unknown* covariance matrices denoted as  $\boldsymbol{\sigma}$ . Here, the covariance matrix depends on the hydrometeors present in the range gate of interest. We assume that the receiver thermal noise is independent of the clutter. On the other hand, the target is considered as a man-made object, which is small (point-like) with respect to the size of the range cell. Hence, the polarimetric scattering matrix of the target is rearranged in a coefficient vector, which is assumed deterministic and *unknown*. Let  $\mathbb{E}\{\mathbf{x}_p\} = \boldsymbol{\mu}$ . Based on the

<sup>1</sup> For a tripole antenna  $L = 3N$ ,  $M = 2N$ ,  $P = 4$ , and  $k = 1$ . For a classical polarization radar using vertical and horizontal linear polarization  $L = 2N$ ,  $M = 2N$ ,  $P = 4$ , and  $k = 1$ .

statistics of the target, clutter, and noise as mentioned above, the received signal vector at the receiver for a moving target, denoted as  $\mathbf{y}_d \in \mathbb{C}^{L \times 1}$  is a complex Gaussian distributed as

$$\begin{aligned} \mathcal{H}_0 : \mathbf{y}_d &\sim \mathcal{CN}(\mathbf{0}, \mathbf{A}\mathbf{S}\mathbf{\Sigma}\mathbf{S}^H\mathbf{A}^H + \sigma\mathbf{I}_L) \\ \mathcal{H}_1 : \mathbf{y}_d &\sim \mathcal{CN}(\mathbf{B}\mathbf{S}\boldsymbol{\mu}, \mathbf{A}\mathbf{S}\mathbf{\Sigma}\mathbf{S}^H\mathbf{A}^H + \sigma\mathbf{I}_L). \end{aligned} \quad (14)$$

Here,  $d$  represents the snapshot index, and  $\mathcal{H}_0$  and  $\mathcal{H}_1$  are hypotheses representing the signal model in the absence and presence of a target, respectively. In (14), we assume that the target follows Swerling-I model, where the target reflectivity remains constant during the dwell time. We denote  $\boldsymbol{\Gamma} = \mathbf{A}\mathbf{S}\mathbf{\Sigma}\mathbf{S}^H\mathbf{A}^H + \sigma\mathbf{I}_L \in \mathbb{C}^{L \times L}$ , which represents the true covariance matrix.

### 3. Target detection with clutter

In this section, we develop a detection test to decide if a target is present in the processed data. In hypothesis testing problems, when both of the density functions are completely known, then the Neyman–Pearson (NP) detector is the uniformly most powerful (UMP) detector. However, in most scenarios, all the parameters of the density function are not known. In such cases, the parameters are modeled as random variables with some density function, and integrated out. This method employs a Bayesian framework to detect a target. Another approach is to use a generalized likelihood ratio test (GLRT), where the parameters are assumed to be deterministic and replaced with their maximum likelihood estimate (MLE). This method may not always be optimal, but it works well in practice. We begin by maximizing the loglikelihood functions under each hypothesis with respect to the unknown parameters.

#### 3.1. Under $\mathcal{H}_0$

Based on (14), the loglikelihood function with respect to the unknown parameters  $\mathbf{S}$  and  $\boldsymbol{\Sigma}$  under the hypothesis  $\mathcal{H}_0$  is expressed as

$$\ln f_0(\boldsymbol{\Sigma}, \mathbf{S}) = -D[L \ln \pi + \ln |\boldsymbol{\Gamma}| + \text{Tr} \{ \boldsymbol{\Gamma}^{-1} \mathbf{R}_0 \}], \quad (15)$$

where  $D$  is the number of snapshots, and  $\mathbf{R}_0$  is the sample covariance matrix under hypothesis  $\mathcal{H}_0$  given as

$$\mathbf{R}_0 = \frac{1}{D} \sum_{d=1}^D \mathbf{y}_d \mathbf{y}_d^H, \quad D \gg L. \quad (16)$$

Let  $\hat{\boldsymbol{\Sigma}}_0$  denote the MLE of  $\boldsymbol{\Sigma}$ . Then,  $\hat{\boldsymbol{\Sigma}}_0$  is given as (see Appendix A),

$$\hat{\boldsymbol{\Sigma}}_0 = (\mathbf{A}\mathbf{S})^\dagger \mathbf{R}_0 (\mathbf{A}\mathbf{S})^{\dagger H} - \sigma (\mathbf{S}^H \mathbf{A}^H \mathbf{A} \mathbf{S}). \quad (17)$$

Replacing  $\boldsymbol{\Sigma}$  in the loglikelihood function with its MLE, we get

$$\ln f_0(\hat{\boldsymbol{\Sigma}}_0, \mathbf{S}) = -D[P + L \ln \pi + (L - P) \ln \sigma + \ln |\mathbf{S}^H \mathbf{A}^H \mathbf{R}_0 \mathbf{A} \mathbf{S}| - \ln |\mathbf{S}^H \mathbf{A}^H \mathbf{A} \mathbf{S}| + \sigma^{-1} \text{Tr} \{ \mathbf{P}_{\text{AS}}^\perp \mathbf{R}_0 \}], \quad (18)$$

where  $\mathbf{P}_{\text{AS}}^\perp$  is a projection matrix expressed as

$$\mathbf{P}_{\text{AS}}^\perp = \mathbf{I}_L - \mathbf{P}_{\text{AS}} = \mathbf{I}_L - \mathbf{A}\mathbf{S}(\mathbf{S}^H \mathbf{A}^H \mathbf{A} \mathbf{S})^{-1} \mathbf{S}^H \mathbf{A}^H. \quad (19)$$

The derivation of the likelihood function in (18) is shown in Appendix A. The sample covariance matrix converges to the true covariance matrix in an asymptotic sense, as the number of snapshots increases [26,27]. In Appendix B, we show that  $\sigma^{-1} \text{Tr} \{ \mathbf{P}_{\text{AS}}^\perp \mathbf{R}_0 \} \approx (L - P)$  for a large number of snapshots. Therefore, the loglikelihood function can be further simplified:

$$\ln f_0(\hat{\boldsymbol{\Sigma}}_0, \mathbf{S}) \approx -D[L + L \ln \pi + (L - P) \ln \sigma + \ln |\mathbf{S}^H \mathbf{A}^H \mathbf{R}_0 \mathbf{A} \mathbf{S}| - \ln |\mathbf{S}^H \mathbf{A}^H \mathbf{A} \mathbf{S}|]. \quad (20)$$

Next, we maximize (20) with respect to  $\mathbf{S}$ . We notice that only the last two terms of (20) are dependent on  $\mathbf{S}$ . The matrix  $\mathbf{A}^H \mathbf{R}_0 \mathbf{A}$  is Hermitian positive definite for  $D \gg L$ . Let  $\mathbf{U}\boldsymbol{\Omega}\mathbf{U}^H$  be the orthogonal factorization of  $\mathbf{A}^H \mathbf{R}_0 \mathbf{A}$ , where  $\mathbf{U}$  contains orthogonal column vectors such that  $\mathbf{U}\mathbf{U}^H = \mathbf{I}_M$ , and  $\boldsymbol{\Omega}$  is a diagonal matrix with eigenvalues of  $\mathbf{A}^H \mathbf{R}_0 \mathbf{A}$  as its diagonal entries, arranged in decreasing order. We partition the orthogonal column vectors of  $\mathbf{U}$  as  $[\mathbf{U}_1 \quad \mathbf{U}_2]$ , such that  $\mathbf{U}_1 \in \mathbb{C}^{M \times P}$ ,  $\mathbf{U}_2 \in \mathbb{C}^{M \times (L-P)}$ . In Appendix C, we show that the MLE of  $\mathbf{S}$ , denoted as  $\hat{\mathbf{S}} = \mathbf{U}_1$ , where  $\mathbf{U}_1$  represents the eigenvectors corresponding to  $P$  largest eigenvalues of  $\mathbf{A}^H \mathbf{R}_0 \mathbf{A}$ . Substituting the MLE of  $\mathbf{S}$  into the loglikelihood function in (20), we get

$$\ln f_0(\hat{\boldsymbol{\Sigma}}_0, \hat{\mathbf{S}}) = -D[L + L \ln \pi + (L - P) \ln \sigma + \ln |\mathbf{U}_1^H \mathbf{A}^H \mathbf{R}_0 \mathbf{A} \mathbf{U}_1| - \ln |\mathbf{U}_1^H \mathbf{A}^H \mathbf{A} \mathbf{U}_1|].$$

The inner product of the delay-Doppler steering matrix  $\mathbf{A}$  and the orthonormal columns of  $\mathbf{U}_1$  is a constant. Hence, the loglikelihood function can be written as

$$\ln f_0(\hat{\boldsymbol{\Sigma}}_0, \hat{\mathbf{S}}) = -D[L + L \ln \pi + (L - P) \ln \sigma + \ln |\mathbf{U}_1^H \mathbf{A}^H \mathbf{R}_0 \mathbf{A} \mathbf{U}_1| - \ln |k\mathbf{I}_P|]. \quad (21)$$

#### 3.2. Under $\mathcal{H}_1$

Following a similar approach, the loglikelihood function with respect to the unknown parameters  $\boldsymbol{\Sigma}$ ,  $\boldsymbol{\mu}$ , and  $\mathbf{S}$  under hypothesis  $\mathcal{H}_1$  in (14), is expressed as

$$\ln f_1(\boldsymbol{\Sigma}, \boldsymbol{\mu}, \mathbf{S}) = -D[L \ln \pi + \ln |\boldsymbol{\Gamma}| + \text{Tr} \{ \boldsymbol{\Gamma}^{-1} \mathbf{R}_1 \}], \quad (22)$$

where  $\mathbf{R}_1$  is the sample covariance matrix under  $\mathcal{H}_1$ , given as

$$\mathbf{R}_1 = \frac{1}{D} \sum_{d=1}^D (\mathbf{y}_d - \mathbf{B}\mathbf{S}\boldsymbol{\mu})(\mathbf{y}_d - \mathbf{B}\mathbf{S}\boldsymbol{\mu})^H, \quad D \gg L. \quad (23)$$

Let  $\hat{\boldsymbol{\Sigma}}_1$  denote the MLE of  $\boldsymbol{\Sigma}$ . Then  $\hat{\boldsymbol{\Sigma}}_1$  is given as (see Appendix A)

$$\hat{\boldsymbol{\Sigma}}_1 = (\mathbf{A}\mathbf{S})^\dagger \mathbf{R}_1 (\mathbf{A}\mathbf{S})^{\dagger H} - \sigma (\mathbf{S}^H \mathbf{A}^H \mathbf{A} \mathbf{S}). \quad (24)$$

Replacing  $\boldsymbol{\Sigma}$  with its MLE in the loglikelihood function, we get

$$\ln f_1(\hat{\boldsymbol{\Sigma}}_1, \boldsymbol{\mu}, \mathbf{S}) = -D[P + L \ln \pi + (L - P) \ln \sigma + \ln |\mathbf{S}^H \mathbf{A}^H \mathbf{R}_1 \mathbf{A} \mathbf{S}| - \ln |\mathbf{S}^H \mathbf{A}^H \mathbf{A} \mathbf{S}| + \sigma^{-1} \text{Tr} \{ \mathbf{P}_{\text{AS}}^\perp \mathbf{R}_1 \}]. \quad (25)$$

Ignoring the scaling parameter and substituting (23), the last term in (25) can be rewritten as

$$\begin{aligned} \text{Tr} \{ \mathbf{P}_{\text{AS}}^\perp \mathbf{R}_1 \} &= \text{Tr} \{ \mathbf{P}_{\text{AS}}^\perp \mathbf{R}_1 \mathbf{P}_{\text{AS}}^\perp \} \\ &= \text{Tr} \{ \mathbf{P}_{\text{AS}}^\perp \mathbf{R}_0 \} - \text{Tr} \{ \mathbf{P}_{\text{AS}}^\perp \bar{\mathbf{y}} \boldsymbol{\mu}^H \mathbf{S}^H \mathbf{B}^H \mathbf{P}_{\text{AS}}^\perp \} \\ &\quad - \text{Tr} \{ \mathbf{P}_{\text{AS}}^\perp \mathbf{B} \mathbf{S} \boldsymbol{\mu} \bar{\mathbf{y}}^H \mathbf{P}_{\text{AS}}^\perp \} + \text{Tr} \{ \mathbf{P}_{\text{AS}}^\perp \mathbf{B} \mathbf{S} \boldsymbol{\mu} \boldsymbol{\mu}^H \mathbf{S}^H \mathbf{B}^H \mathbf{P}_{\text{AS}}^\perp \} \\ &\quad + \text{Tr} \{ \mathbf{P}_{\text{AS}}^\perp \bar{\mathbf{y}} \bar{\mathbf{y}}^H \mathbf{P}_{\text{AS}}^\perp \} - \text{Tr} \{ \mathbf{P}_{\text{AS}}^\perp \bar{\mathbf{y}} \bar{\mathbf{y}}^H \mathbf{P}_{\text{AS}}^\perp \} \end{aligned} \quad (27)$$

where  $\bar{\mathbf{y}} = (1/D) \sum_{d=1}^D \mathbf{y}_d$ . In (26) we used the idempotent property of a project matrix, and in (27) we add and subtract  $\text{Tr} \{ \mathbf{P}_{\text{AS}}^\perp \bar{\mathbf{y}} \bar{\mathbf{y}}^H \mathbf{P}_{\text{AS}}^\perp \}$ . Rewriting (27) in compact form we get

$$\text{Tr} \{ \mathbf{P}_{\text{AS}}^\perp \mathbf{R}_1 \} = \text{Tr} \{ \mathbf{P}_{\text{AS}}^\perp (\mathbf{R}_0 - \bar{\mathbf{y}} \bar{\mathbf{y}}^H) \} + \text{Tr} \{ \mathbf{P}_{\text{AS}}^\perp (\bar{\mathbf{y}} - \mathbf{B}\mathbf{S}\boldsymbol{\mu}) (\bar{\mathbf{y}} - \mathbf{B}\mathbf{S}\boldsymbol{\mu})^H \} \quad (28)$$

$$\approx \text{Tr} \{ \mathbf{P}_{\text{AS}}^\perp (\mathbf{R}_0 - \bar{\mathbf{y}} \bar{\mathbf{y}}^H) \} = \text{Tr} \{ \mathbf{P}_{\text{AS}}^\perp \mathbf{R}_2 \} \quad (29)$$

where  $\mathbf{R}_2 \triangleq (\mathbf{R}_0 - \bar{\mathbf{y}} \bar{\mathbf{y}}^H) = (1/D) \sum_{d=1}^D (\mathbf{y}_d - \bar{\mathbf{y}})(\mathbf{y}_d - \bar{\mathbf{y}})^H$ . For large number of snapshots, the sample mean  $\bar{\mathbf{y}}$  and the sample covari-

ance matrix  $\mathbf{R}_2$  converges in probability to true mean and true covariance [26, Chapter 2], i.e.,  $\bar{\mathbf{y}} \rightarrow \mathbf{B}\mathbf{S}\boldsymbol{\mu}$  and  $\mathbf{R}_2 \rightarrow \boldsymbol{\Gamma}$ . Therefore, the last term in (28) goes to zero for large number of snapshots. Then, the loglikelihood function is given as

$$\ln f_1(\hat{\boldsymbol{\Sigma}}_1, \boldsymbol{\mu}, \mathbf{S}) \approx -D[P + L \ln \pi + (L - P) \ln \sigma + \ln |\mathbf{S}^H \mathbf{A}^H \mathbf{R}_1 \mathbf{A}\mathbf{S}| - \ln |\mathbf{S}^H \mathbf{A}^H \mathbf{A}\mathbf{S}| + \sigma^{-1} \text{Tr} \{ \mathbf{P}_{\text{AS}}^\perp \mathbf{R}_2 \}]. \quad (30)$$

Considering again the trace approximation for the last term in (30) (see Appendix B), the loglikelihood function becomes

$$\ln f_1(\hat{\boldsymbol{\Sigma}}_1, \boldsymbol{\mu}, \mathbf{S}) \approx -D[L + L \ln \pi + (L - P) \ln \sigma + \ln |\mathbf{S}^H \mathbf{A}^H \mathbf{R}_1 \mathbf{A}\mathbf{S}| - \ln |\mathbf{S}^H \mathbf{A}^H \mathbf{A}\mathbf{S}|]. \quad (31)$$

Next, we maximize (31) with respect to  $\boldsymbol{\mu}$ . As can be seen from (31), only the fourth term depends on  $\boldsymbol{\mu}$ . The MLE of  $\boldsymbol{\mu}$  is given as (see Appendix D)

$$\hat{\boldsymbol{\mu}} = (\mathbf{B}\mathbf{S})^\dagger \bar{\mathbf{y}} \quad (32)$$

Substituting (32) into (23), we get

$$\mathbf{R}_1 = \frac{1}{D} \sum_{d=1}^D (\mathbf{y}_d - \mathbf{P}_{\text{BS}} \bar{\mathbf{y}})(\mathbf{y}_d - \mathbf{P}_{\text{BS}} \bar{\mathbf{y}})^H = \mathbf{R}_2 + \mathbf{P}_{\text{BS}}^\perp \bar{\mathbf{y}} \bar{\mathbf{y}}^H \mathbf{P}_{\text{BS}}^\perp \quad (33)$$

Using (33), we further simplify the expression  $\ln |\mathbf{S}^H \mathbf{A}^H \mathbf{R}_1 \mathbf{A}\mathbf{S}|$  as follows:

$$\begin{aligned} \ln |\mathbf{S}^H \mathbf{A}^H \mathbf{R}_1 \mathbf{A}\mathbf{S}| &= \ln |\mathbf{S}^H \mathbf{A}^H (\mathbf{R}_2 + \mathbf{P}_{\text{BS}}^\perp \bar{\mathbf{y}} \bar{\mathbf{y}}^H \mathbf{P}_{\text{BS}}^\perp) \mathbf{A}\mathbf{S}| \\ &= \ln \left( 1 + \bar{\mathbf{y}}^H \mathbf{P}_{\text{BS}}^\perp \mathbf{A}\mathbf{S} (\mathbf{S}^H \mathbf{A}^H \mathbf{R}_2 \mathbf{A}\mathbf{S})^{-1} \mathbf{S}^H \mathbf{A}^H \mathbf{P}_{\text{BS}}^\perp \bar{\mathbf{y}} \right) \\ &\quad + \ln |\mathbf{S}^H \mathbf{A}^H \mathbf{R}_2 \mathbf{A}\mathbf{S}| \end{aligned} \quad (34)$$

$$\approx \ln |\mathbf{S}^H \mathbf{A}^H \mathbf{R}_2 \mathbf{A}\mathbf{S}| \quad (35)$$

where, in (34) we used the determinant identity in [28, Theorem 13.3.8], and the approximation in (35) is due to the convergence of sample mean to true mean in probability, for large number of snapshots, i.e.,  $\mathbf{P}_{\text{BS}}^\perp \bar{\mathbf{y}} \rightarrow \mathbf{P}_{\text{BS}}^\perp \mathbf{B}\mathbf{S}\boldsymbol{\mu} = \mathbf{0}$ . Hence, the loglikelihood function obtained after substituting the MLE of  $\boldsymbol{\mu}$  is given as

$$\ln f_1(\hat{\boldsymbol{\Sigma}}_1, \hat{\boldsymbol{\mu}}, \mathbf{S}) \approx -D[L + L \ln \pi + (L - P) \ln \sigma + \ln |\mathbf{S}^H \mathbf{A}^H \mathbf{R}_2 \mathbf{A}\mathbf{S}| - \ln |\mathbf{S}^H \mathbf{A}^H \mathbf{A}\mathbf{S}|]. \quad (36)$$

We maximize (36) with respect to  $\mathbf{S}$ , following similar steps as we did for hypothesis  $\mathcal{H}_0$ . Let  $\mathbf{V}\boldsymbol{\Upsilon}\mathbf{V}^H$  be the orthogonal factorization of  $\mathbf{A}^H \mathbf{R}_2 \mathbf{A}$ , where  $\mathbf{V}$  represents the orthogonal column vectors such that  $\mathbf{V}\mathbf{V}^H = \mathbf{I}_M$ , and  $\boldsymbol{\Upsilon}$  is a diagonal matrix with eigenvalues of  $\mathbf{A}^H \mathbf{R}_2 \mathbf{A}$  as its diagonal entries, arranged in descending order. We partition the orthogonal column vectors of  $\mathbf{V}$  as  $[\mathbf{V}_1 \quad \mathbf{V}_2]$ , such that  $\mathbf{V}_1 \in \mathbb{C}^{M \times P}$ ,  $\mathbf{V}_2 \in \mathbb{C}^{M \times (L-P)}$ . Then, the MLE of  $\mathbf{S}$  is given as  $\mathbf{V}_1$  (see Appendix C), where  $\mathbf{V}_1$  represents the eigenvectors corresponding to the  $P$  largest eigenvalues of  $\mathbf{A}^H \mathbf{R}_2 \mathbf{A}$ . Substituting the MLE of  $\mathbf{S}$  into the loglikelihood function, we get

$$\ln f_1(\hat{\boldsymbol{\Sigma}}_1, \hat{\boldsymbol{\mu}}, \hat{\mathbf{S}}) = -D[L + L \ln \pi + (L - P) \ln \sigma + \ln |\mathbf{V}_1^H \mathbf{A}^H \mathbf{R}_2 \mathbf{A}\mathbf{V}_1| - \ln |k\mathbf{I}_P|]. \quad (37)$$

### 3.3. GLRT detector

The GLRT detector is written as

$$\begin{aligned} \max_{\{\boldsymbol{\Sigma}, \boldsymbol{\mu}, \mathbf{S}\}} \ln f_1(\boldsymbol{\Sigma}, \boldsymbol{\mu}, \mathbf{S}) - \max_{\{\boldsymbol{\Sigma}, \mathbf{S}\}} \ln f_0(\boldsymbol{\Sigma}, \mathbf{S}) \\ = \ln f_1(\hat{\boldsymbol{\Sigma}}_1, \hat{\boldsymbol{\mu}}, \hat{\mathbf{S}}) - \ln f_0(\hat{\boldsymbol{\Sigma}}_0, \hat{\mathbf{S}}) \geq \ln \kappa. \end{aligned} \quad (38)$$

Substituting (21) and (37) into (38), the GLRT is given as

$$D[\ln |\mathbf{U}_1^H \mathbf{A}^H \mathbf{R}_0 \mathbf{A}\mathbf{U}_1| - \ln |\mathbf{V}_1^H \mathbf{A}^H \mathbf{R}_2 \mathbf{A}\mathbf{V}_1|] \geq \ln \kappa. \quad (39)$$

Using (29) and [28, Theorem 13.3.8], the first term in (39) can be written as

$$\begin{aligned} \ln |\mathbf{U}_1^H \mathbf{A}^H \mathbf{R}_0 \mathbf{A}\mathbf{U}_1| &= \ln |\mathbf{U}_1^H \mathbf{A}^H (\mathbf{R}_2 + \bar{\mathbf{y}} \bar{\mathbf{y}}^H) \mathbf{A}\mathbf{U}_1| \\ &= \ln \left( 1 + \bar{\mathbf{y}}^H \mathbf{A}\mathbf{U}_1 (\mathbf{U}_1^H \mathbf{A}^H \mathbf{R}_2 \mathbf{A}\mathbf{U}_1)^{-1} \mathbf{U}_1^H \mathbf{A}^H \bar{\mathbf{y}} \right) \\ &\quad + \ln |\mathbf{U}_1^H \mathbf{A}^H \mathbf{R}_2 \mathbf{A}\mathbf{U}_1|. \end{aligned} \quad (40)$$

Substituting (40) in (39), the GLRT can be rewritten as

$$\begin{aligned} D \left[ \ln \left( 1 + \bar{\mathbf{y}}^H \mathbf{A}\mathbf{U}_1 (\mathbf{U}_1^H \mathbf{A}^H \mathbf{R}_2 \mathbf{A}\mathbf{U}_1)^{-1} \mathbf{U}_1^H \mathbf{A}^H \bar{\mathbf{y}} \right) \right. \\ \left. + \ln |\mathbf{U}_1^H \mathbf{A}^H \mathbf{R}_2 \mathbf{A}\mathbf{U}_1| - \ln |\mathbf{V}_1^H \mathbf{A}^H \mathbf{R}_2 \mathbf{A}\mathbf{V}_1| \right] \geq \ln \kappa. \end{aligned} \quad (41)$$

The distribution of the GLRT statistic for the measurement model does not have a closed-form expression for a finite number of snapshots. Hence, we explore the asymptotic performance characteristics of the GLRT statistic. The matrices  $\mathbf{U}_1$  and  $\mathbf{V}_1$  represent the eigenvectors corresponding to the  $P$  largest eigenvalues of  $\mathbf{A}^H \mathbf{R}_0 \mathbf{A}$  and  $\mathbf{A}^H \mathbf{R}_2 \mathbf{A}$ , respectively. When we have a large number of snapshots, both  $\mathbf{R}_0$  and  $\mathbf{R}_2$  converge to the true covariance matrix,  $\boldsymbol{\Gamma}$ . Note that the true covariance matrix of the observation vector under each hypothesis is the same. Hence, the eigenvectors corresponding to  $P$  largest eigenvalues of  $\mathbf{A}^H \mathbf{R}_0 \mathbf{A}$  and  $\mathbf{A}^H \mathbf{R}_2 \mathbf{A}$  also converge. Based on this asymptotic property of sample covariance matrix we replace  $\mathbf{V}_1$  with  $\mathbf{U}_1$  in (41). Then, the GLRT statistic can be written as

$$D \left[ \ln \left( 1 + \bar{\mathbf{y}}^H \mathbf{A}\mathbf{U}_1 (\mathbf{U}_1^H \mathbf{A}^H \mathbf{R}_2 \mathbf{A}\mathbf{U}_1)^{-1} \mathbf{U}_1^H \mathbf{A}^H \bar{\mathbf{y}} \right) \right] \geq \ln \kappa. \quad (42)$$

Let  $\mathbf{z}_d = \mathbf{U}_1^H \mathbf{A}^H \mathbf{y}_d$ . Then the mean of the random variable  $\mathbf{z}_d$  is  $\mathbf{U}_1^H \mathbf{A}^H \mathbf{B}\mathbf{S}\boldsymbol{\mu}$  and the covariance is  $\mathbf{U}_1^H \mathbf{A}^H \boldsymbol{\Gamma} \mathbf{A}\mathbf{U}_1$ . The new sample mean and sample covariance are  $\bar{\mathbf{z}} = (1/D) \sum_{d=1}^D \mathbf{z}_d$  and  $\mathbf{R}_z = (1/D) \sum_{d=1}^D (\mathbf{z}_d - \bar{\mathbf{z}})(\mathbf{z}_d - \bar{\mathbf{z}})^H$ , respectively. Hence, the decision test statistic in (42) is given as

$$D \ln \left( 1 + \bar{\mathbf{z}}^H \mathbf{R}_z^{-1} \bar{\mathbf{z}} \right) \geq \ln \kappa. \quad (43)$$

Removing the logarithm and ignoring the constant term, the equivalent test statistic is

$$\xi = \bar{\mathbf{z}}^H \mathbf{R}_z^{-1} \bar{\mathbf{z}}. \quad (44)$$

### 3.4. Distribution of test statistic

We present the probability density function of the test statistic in (44) for the bistatic scenario under both  $\mathcal{H}_0$  and  $\mathcal{H}_1$ . It follows from [29, Corollary 5.2.1], that the test statistic follows a F-distribution denoted by  $\mathcal{F}_{\nu_1, \nu_2}(\lambda)$ , where,  $\nu_1 = 2P$  and  $\nu_2 = 2(D - P)$  represents degrees of freedom, and  $\lambda$  is the non-centrality parameter. The factor 2 in the expressions of the degree of freedom takes into account that the data is complex. The test statistic in (44) is distributed as follows:

$$\frac{2(D - P)}{2P} \xi \sim \begin{cases} \mathcal{F}_{2P, 2(D-P)}, & \text{under } \mathcal{H}_0 \\ \mathcal{F}_{2P, 2(D-P)}(\lambda), & \text{under } \mathcal{H}_1 \end{cases}. \quad (45)$$

In the derivation of the test statistic in (44), we considered a large number of snapshots. As the number of snapshots  $D$  increases, the degrees of freedom  $\nu_2$  also increases, and the F-distribution  $\mathcal{F}_{\nu_1, \nu_2}$  can be approximated as a chi-square distribution denoted by  $\chi_{\nu_1}^2$  [30, Chapter 2]. The distribution of the test statistic in (45) can be expressed as

$$2(D - P) \xi \sim \begin{cases} \chi_{2P}^2, & \text{under } \mathcal{H}_0 \\ \chi_{2P}^2(\lambda), & \text{under } \mathcal{H}_1 \end{cases}, \quad (46)$$

where the non-centrality parameter is given as [29, Corollary 5.2.1]

$$\lambda = 2D \boldsymbol{\mu}^H \mathbf{S}^H \mathbf{B}^H \mathbf{A}\mathbf{U}_1 [\mathbf{U}_1^H \mathbf{A}^H \boldsymbol{\Gamma} \mathbf{A}\mathbf{U}_1]^{-1} \mathbf{U}_1^H \mathbf{A}^H \mathbf{B}\mathbf{S}\boldsymbol{\mu} \quad (47)$$

The non-centrality parameter depends on the transmitted signal, the target scattering coefficients, the covariance of clutter, and the receiver noise. The exact detection performance is given by  $P_{FA} = Q_{\chi_{2P}^2}(\delta)$ , where  $\delta$  is the detection threshold for a given probability of false alarm, and  $Q_{\chi_{2P}^2}$  is the right-tail probability for a chi-squared distribution with  $2P$  degrees of freedom. In addition, the expression of  $P_{FA}$  does not depend on the transmitted signal, clutter, and noise, indicating the CFAR of the detector. The probability of detection,  $P_D = Q_{\chi_{2P}^2(\lambda)}(\delta)$ , where  $Q_{\chi_{2P}^2(\lambda)}$  is the right-tail probability of a random variable with a non-central chi-squared distribution with  $2P$  degrees of freedom (see [30]). The proposed detection test does not require secondary data to estimate the clutter parameters. The unknown parameters are estimated by using only the data that correspond to the range gate of interest. Hence, the performance of the test would not be affected if the clutter is spatially inhomogeneous.

In case of a stationary target, we observe no Doppler shift from the target. Assuming that the delay observed from the target and clutter are approximately the same, i.e.,  $n_p \approx n_c$ , the observed delay-Doppler matrix  $\mathcal{D}_{n_p,0} \approx \mathcal{D}_{n_c,0}$ . Due to this assumption, we can replace  $\mathbf{B}$  with  $\mathbf{A}$  in the expression of the non-centrality parameter in (47). On further simplifying (47) by expanding  $\mathbf{\Gamma}$  and replacing  $\mathbf{S}$  with its MLE,  $\mathbf{U}_1$ , the estimated non-centrality parameter of a stationary target, which is denoted by  $\hat{\lambda}$ , is given as

$$\hat{\lambda} = 2k^2 D \boldsymbol{\mu}^H \left[ k^2 \boldsymbol{\Sigma} + k\sigma \mathbf{I}_P \right]^{-1} \boldsymbol{\mu} = \frac{2D}{\sigma} \left[ \boldsymbol{\mu}^H \left( \frac{\boldsymbol{\Sigma}}{\sigma} + \frac{1}{k} \mathbf{I}_P \right)^{-1} \boldsymbol{\mu} \right]. \quad (48)$$

The expression of the non-centrality parameter in (48) is a weighted inner product of the target scattering coefficients, where the weights depend on the number of snapshots, clutter covariance, and the receiver noise. In the absence of clutter, the expression in (48) simplifies to a simple energy-based detector [30, Chapter 7].

In the proposed signal model, we assumed a hypothesized target to be present in the range cell of interest. Therefore, at every range cell, the test statistic in (44) is to be computed for a range of target delay and Doppler values, building a bank of detectors. However, computing the test statistic in (44) is not computationally expensive. It involves computing the singular value decomposition of an  $M \times M$  Hermitian symmetric matrix, where  $M = 2N$  depends on the sampling rate of the receiver, and inverting a  $P \times P$  matrix, where  $P \leq 4$  depends on the number of polarization channels considered in the signal model.

#### 4. Numerical simulations

In this section, we illustrate the performance of our proposed detector presented in Section 3. For simplicity, we consider a 2-D scenario, where both the receiver and target are in the same plane. Our analysis can be easily extended to a 3-D scenario. In our simulation setup, we consider a dual-polarized weather radar (WSR-88D) [16] as our signal of opportunity. The WSR-88D is a pulse-Doppler system that measures three primary characteristics of the radar echoes: reflectivity, Doppler (radial) velocity, and width of the Doppler spectrum. Parameters such as range of observation, number of pulses averaged, and range resolution vary depending on the characteristics of interest [16, Appendix A]. The transmitter is attached to a platform rotating at a constant rotation rate. The signal parameters of the transmitted signal are listed in Table 1.

The transmitter, target, and the receiver are located in the  $x - y$  plane, and consequently the elevation angle of the receiver is set to  $\theta = 0$ . In our simulations, we consider the transmitter to be located at  $(-3.46 \text{ km}, 2 \text{ km})$  and an EMVS receiver located at  $(3.46 \text{ km}, 2 \text{ km})$ . Let  $\tau$  represent the pulse width of the complex

**Table 1**

Dual-polarized transmitter specifications with velocity as the characteristic of interest.

Parameter	Value
Carrier frequency	2.7 GHz
Bandwidth	0.63 MHz
Beam width	0.96°
Pulse width	1.5 $\mu$ s (short pulse)
Pulse repetition frequency	322 – 1282 Hz
Range of Observation	230 km (for velocity)
Range resolution	250 ms (for velocity)
Orientation and ellipticity	$(\pi/4, 0)$ and $(-\pi/4, 0)$

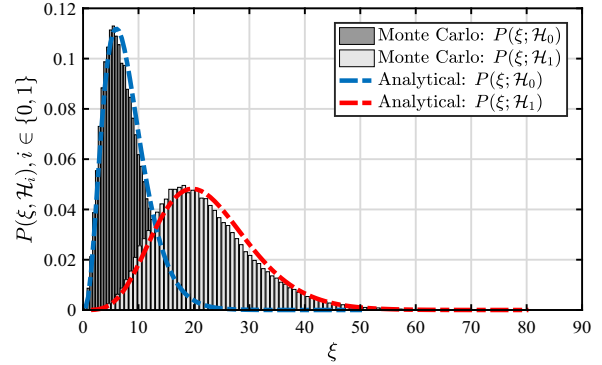


**Fig. 1.** Normalized histogram (empirical PDF) and the analytic PDF under  $\mathcal{H}_0$  and  $\mathcal{H}_1$ , with SNR =  $-10$  dB, CNR =  $10$  dB, number of samples per snapshot  $N = 8$ , and number of snapshots  $D = 200$ .

envelope signal  $s(t)$ , with no phase or frequency modulation. Then, based on the Nyquist sampling criterion, the sampling frequency denoted by  $f_s = 2/\tau$ . However, in our signal model, we collect  $N/2$  samples from each polarization at a single range cell, which requires the receiver to operate at a sampling rate of  $f_s = 1/\Delta t = N/\tau$ . The target is illuminated by the weather radar and the scattering coefficients of the target depend on the azimuth view angle of the receiver. In our simulation, we assume the target to be located at the origin, moving with a velocity of  $30 \text{ m/s}$  in the positive  $y$ -axis direction. Due to this, we set the azimuth angle of the receiver to  $\phi = \pi/6$ . The velocity of the target lies within the range of maximum Doppler radial velocity that can be measured by a weather radar (for WSR-88D the maximum Doppler unambiguous radial velocity is  $32 \text{ m/s}$ ). The received signal contains reflections from the target and the stationary clutter surrounding the target. In addition, we use the following definitions of signal-to-noise ratio (SNR) and clutter-to-noise ratio (CNR) in our simulation results:

$$\text{SNR (in dB)} = 10 \log_{10} \frac{\boldsymbol{\mu}^H \mathbf{S}^H \mathbf{S} \boldsymbol{\mu}}{\sigma} \quad (49)$$

$$\text{CNR (in dB)} = 10 \log_{10} \frac{\text{Tr}\{\boldsymbol{\Sigma}\}}{\sigma}. \quad (50)$$

The target scattering coefficients are generated from a  $\mathcal{CN}(0, 1)$  distribution. Similarly, the entries of the clutter covariance matrix are generated from a  $\mathcal{CN}(0, 1)$  distribution, and then scaled to satisfy the required SNR and CNR, respectively.

##### 4.1. Distribution of the test statistic

We now validate the distribution of the test statistic obtained for the GLRT detector described in Section 3. Fig. 1 shows the empirical distribution and the analytic distribution of the detector test statistic under each hypothesis, in the presence of clutter. In our simulation, the target scattering coefficients and the transmitted signal were generated randomly, and fixed, such that

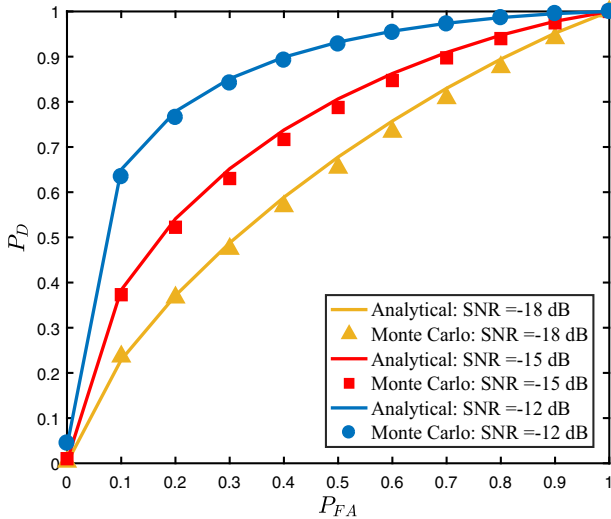


**Fig. 2.** ROC curves for different values of SNR. The solid line plot and the scattered plot indicate the probability of detection obtained from the analytical distribution and the empirical distribution, respectively.

SNR = -10 dB. The number of samples in each snapshot  $N = 8$  and the number of snapshots  $D = 200$ . Note that in our definition of snapshot, we sample two pulses of different polarization. We plot the normalized histogram generated from  $10^5$  Monte Carlo runs of the test statistic in (44), by randomly generating clutter scattering coefficients in each run, such that CNR = 10 dB. As shown in Fig. 1, the empirical distribution closely matches the analytic distribution obtained in (46).

#### 4.2. Detector performance

In this section, we demonstrate the sensitivity of the proposed detector. In Fig. 2, we plot the receiver operating characteristic (ROC) for 100 different realizations of the test statistic in (44). The ROC curve is obtained by taking the average of the probability of detection for 100 different realizations of  $\mu$ ,  $\Sigma$ , and  $S$ . The probability of detection for the empirical distribution is computed from the normalized histogram plot obtained from  $10^5$  Monte Carlo runs of the test statistic in (44), by randomly generating clutter scattering coefficients in each run, such that CNR = 10 dB. The performance of the detector improves as the SNR increases.

In Fig. 3, we demonstrate the performance of the detector for a moving target and a stationary target. Here, we select CNR = 10 dB,  $N = 8$ ,  $D = 200$ , and plot the probability of detection for 50 different realizations of  $\mu$ ,  $\Sigma$ , and  $S$ . For a moving target, we consider the target to be present at a distance of 100 ms offset in the negative  $y$ -axis direction from the center of the range cell under consideration located at origin, and moving with a velocity of 10 m/s in positive  $y$ -axis direction. Due to this assumption,  $n_p \neq n_c$ , and correspondingly the entries of the inner product of  $B^H A$  in the expression of the non-centrality parameter in (47) are not close to Identity matrix. For a stationary target, we consider the target to be present in the center of the range cell under test. Therefore, for a stationary target,  $n_p = n_c$ , and correspondingly the inner product of  $B^H A$  is equal to  $kI_M$ . Thus, the probability of detection, which depends on the system settings through the non-centrality parameter is larger for a stationary target. We note that, under certain conditions, the entries of the inner product of  $B^H A$  are close to Identity matrix even in the case of a moving target. For example, when the target is in the center of the range cell, then  $n_p = n_c$ . Then, the inner product of  $B^H A$  is given as

$$(\mathcal{D}_{n_c, \omega_D} \otimes \mathbf{D}_{\theta, \phi})^H (\mathcal{D}_{n_c, 0} \otimes \mathbf{D}_{\theta, \phi}) = (\mathcal{D}_{n_c, \omega_D}^H \mathcal{D}_{n_c, 0} \otimes kI_M)$$

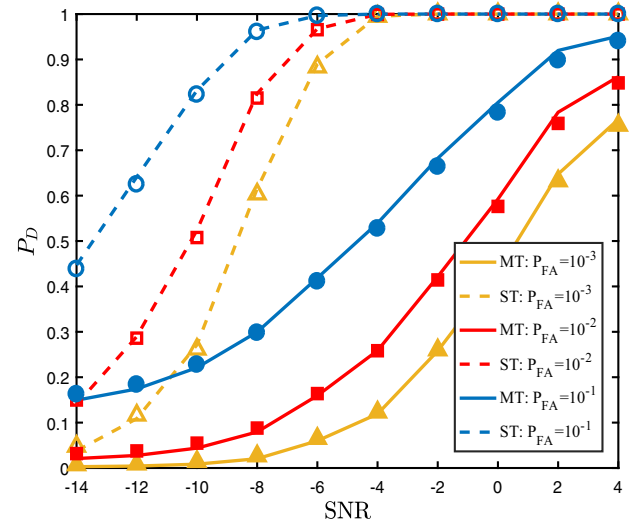


**Fig. 3.** Probability of detection curves across different values of SNR values keeping the probability of false alarm constant. The solid line plot and the dashed line plot indicate the probability of detection obtained from the analytical distribution for a moving (MT) and a stationary target (ST), respectively. The scatter plots outlining the solid and dashed line curves indicate the probability of detection obtained from the empirical distribution for the given value of probability of false alarm.

where

$$\mathcal{D}_{n_c, \omega_D}^H \mathcal{D}_{n_c, 0} = \mathbf{F}_N^H \mathbf{L}_N(2\pi n_c/N) \mathbf{F}_N \mathbf{L}_N^H(\omega_D) \mathbf{L}_N(0) \mathbf{F}_N^H \mathbf{L}_N(-2\pi n_c/N) \mathbf{F}_N.$$

If the entries of the diagonal matrix  $\mathbf{L}_N^H(\omega_D)$  are close to one, then  $B^H A$  will be close to Identity matrix. In such scenarios, the probability of detection is approximately the same for a moving target and a stationary target using the proposed approach.

Next, we looked at the performance of the detector under varying CNR values for a target located at the center of the range cell moving with a velocity of 30 m/s in positive  $y$ -axis direction. For a weather radar, depending on the hydrometeor present in a given range gate, the clutter intensity varies accordingly [18, Chapter 7]. In Fig. 4a and b, we plot the probability of detection for 100 different realizations of  $\mu$ ,  $\Sigma$ , and  $S$ , across a wide range of SNR and CNR values. We keep the probability of false alarm fixed at  $P_{FA} = 10^{-3}$ , number of samples per snapshot  $N = 8$ , and the number of snapshots  $D = 200$  constant, across different SNR and CNR values. We observe that the detector performance under both analytical and empirical distribution match closely. Further, we notice a transition phase at SNR = -10 dB, for both analytical and empirical, probability of detection plots.

In Fig. 5, which addresses target detection of an active radar and assumes complete knowledge of the signal information matrix  $S$ . We call this detector the oracle detector. Also, in [22]  $A = B$ , therefore, in the simulation environment, we consider a hypothesized stationary target present in the center of the range cell of interest. Here, we select CNR = 5 dB,  $N = 8$ , and  $D = 500$ . The dashed lines indicate the probability of detection for a given probability of false alarm across different values of SNR obtained from Hurtado and Nehorai [22, Eq. (24)], where the complete knowledge of the signal information matrix,  $S$ , is known at the receiver. The solid lines indicate the probability of detection obtained from (46), where the signal information matrix,  $S$  is estimated from the signal-dependent clutter  $\Gamma$ . It can be seen that the proposed detector closely matches the performance of the oracle detector, however, it is important to note that the oracle detector in [22] does not require large number of snapshots.

Finally, we looked at the performance of the detector under different number of snapshots. In the proposed model, the signal subspace is unknown and is estimated from the covariance ma-

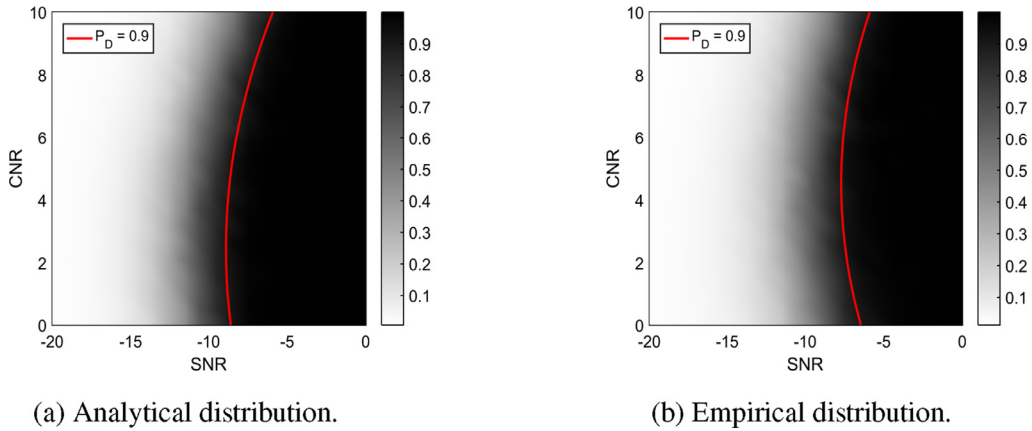


**Fig. 4.** Probability of detection for different values of SNR and CNR. The probability of false alarm is fixed at  $10^{-3}$ . The number of samples per snapshot  $N = 8$  and number of snapshots  $D = 200$ . The probability of detection is represented using gray scale pixels, where the darker pixels indicate higher values of probability of detection.

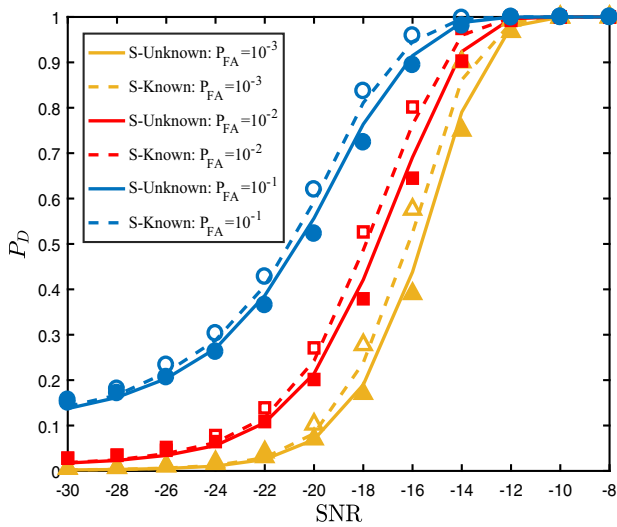


**Fig. 5.** Probability of detection curves across different values of SNR values keeping the probability of false alarm constant. The solid line plot and the dashed line plot indicate the probability of detection obtained from the analytical distribution for stationary target when the signal information matrix is known and unknown, respectively. The filled and hollow marker scatter plots outlining the solid and dashed line curves indicate the probability of detection obtained from the empirical distribution for unknown and known signal information matrix, respectively.

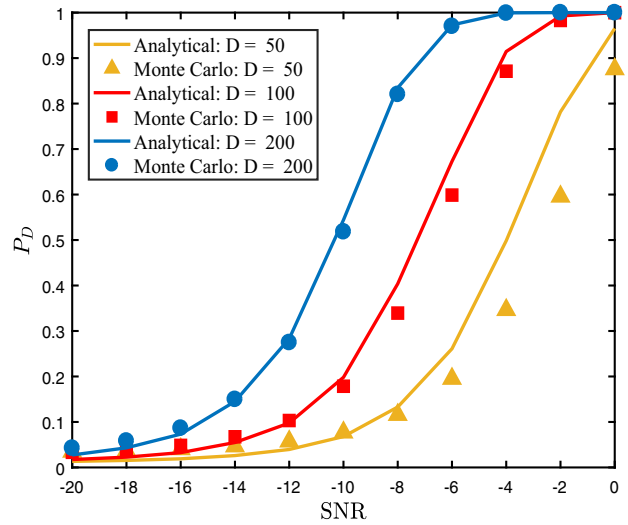


**Fig. 6.** Probability of detection curves across different SNR values for varying number of snapshots. The solid line plot and the scattered plot indicate the probability of detection obtained from the analytical distribution and the empirical distribution, respectively. The number of samples per snapshot  $N = 8$  and number of snapshots  $D = \{50, 100, 200\}$ , with a background CNR = 10 dB.

trix of the recorded data contaminated with clutter. When we have small number of snapshots, the expression of the test statistic in (41) cannot be simplified to (42), due to which the test statistic does not follow a chi-square distribution. To demonstrate this, we keep the simulation environment same as the previous experiment and only vary the number of snapshots. In Fig. 6, we notice that the performance of the detector improves as the number of snapshots increases. The proposed detectors in (44) is an energy detectors. As the number of snapshots increases, the integration time to compute the probability of detection increases, thereby improving the performance of the detector.

## 5. Conclusions

In this work, we presented a GLRT-based detector for a passive radar network using EMVS, with weather radar as signal of opportunity, when the direct path signal from the transmitter is not available. We considered the effect of signal-dependent clutter in the surveillance channel, and derived a GLRT detector for a bistatic scenario. The exact distribution of the test statistic under the hy-

pothesis is presented. The CFAR property of the detector is demonstrated in (44), where the expression of the test statistic under the null-hypothesis is not dependent on the transmitted signal, clutter, and noise. Using numerical simulations, the analytic expressions of the detector test-statistic under different settings are validated. Furthermore, we studied the performance of the proposed detector in different bistatic scenarios, by varying the network settings such as, number of snapshots, SNR, and CNR.

In the future, we will consider a passive multistatic system formed by several receivers. Then, we will develop a centralized approach for target detection in the presence of inhomogeneous signal-dependent clutter. We will also address passive radar networks in the presence of multiple transmitters of opportunity. In addition, we will extend our analysis to multi-target and extended target scenario in a passive radar network.

## Appendix A. MLE of the clutter covariance matrix

Here, we derive the MLE of the unknown clutter covariance matrix of the concentrated loglikelihood functions in (15) and (22) using the results of [31, Theorem 1.1] and [22]. The concentrated log-

likelihood function under hypothesis  $\mathcal{H}_i$ , where  $i \in \{0, 1\}$  indicates the hypothesis, is given by

$$\ln f_i(\boldsymbol{\Sigma}) = -D \left[ L \ln \pi + \ln |\boldsymbol{\Gamma}| + \text{Tr} \left\{ \boldsymbol{\Gamma}^{-1} \mathbf{R} \right\} \right] \quad (\text{A.1})$$

where  $\mathbf{R}$  represents the corresponding sample covariance matrix. Let  $\hat{\boldsymbol{\Sigma}}$  be the MLE of  $\boldsymbol{\Sigma}$ , then based on [31, Theorem 1.1, Eq. (8)]

$$\hat{\boldsymbol{\Sigma}} = (\mathbf{AS})^\dagger \mathbf{R} (\mathbf{AS})^{\dagger H} - \sigma (\mathbf{S}^H \mathbf{A}^H \mathbf{AS}). \quad (\text{A.2})$$

Substituting  $\hat{\boldsymbol{\Sigma}}$  in (A.1) and further simplifying, we get [31, Eq. (24)]

$$\begin{aligned} \ln f_i(\hat{\boldsymbol{\Sigma}}) = & -D \left[ P + L \ln \pi + \ln |\mathbf{S}^H \mathbf{A}^H \mathbf{AS}| + (L - P) \ln \sigma \right. \\ & \left. + \ln \left| (\mathbf{AS})^\dagger \mathbf{R} (\mathbf{AS})^{\dagger H} \right| + \sigma^{-1} \text{Tr} \left\{ \mathbf{P}_{\text{AS}}^\perp \mathbf{R} \right\} \right]. \end{aligned} \quad (\text{A.3})$$

Expanding the fifth term in (A.3) and further simplifying we get the following expression of the loglikelihood function:

$$\begin{aligned} \ln f_i(\hat{\boldsymbol{\Sigma}}) = & -D \left[ P + L \ln \pi - \ln |\mathbf{S}^H \mathbf{A}^H \mathbf{AS}| + (L - P) \ln \sigma \right. \\ & \left. + \ln |\mathbf{S}^H \mathbf{A}^H \mathbf{RAS}| + \sigma^{-1} \text{Tr} \left\{ \mathbf{P}_{\text{AS}}^\perp \mathbf{R} \right\} \right] \end{aligned} \quad (\text{A.4})$$

## Appendix B. Trace approximation

In this Appendix, we show that  $\sigma^{-1} \text{Tr} \left\{ \mathbf{P}_{\text{AS}}^\perp \mathbf{R} \right\}$ , where  $\mathbf{R}$  is a sample covariance matrix of the hypothesis under consideration, goes to a finite value when we consider a large number of snapshots. Using asymptotic statistics, it can be shown that the sample covariance matrix converges to the true covariance for a large number of snapshots [26, Chapter 2]. We replace the sample covariance matrix  $\mathbf{R}$  in  $\sigma^{-1} \text{Tr} \left\{ \mathbf{P}_{\text{AS}}^\perp \mathbf{R} \right\}$  with  $\boldsymbol{\Gamma}$ , and then expand as follows:

$$\begin{aligned} \sigma^{-1} \text{Tr} \left\{ \mathbf{P}_{\text{AS}}^\perp \mathbf{R} \right\} & \approx \sigma^{-1} \text{Tr} \left\{ \mathbf{P}_{\text{AS}}^\perp \boldsymbol{\Gamma} \right\}, \quad \text{for } D \gg L \\ & = \sigma^{-1} \text{Tr} \left\{ \boldsymbol{\Gamma} - \mathbf{P}_{\text{AS}} \boldsymbol{\Gamma} \right\}. \end{aligned} \quad (\text{B.1})$$

Expanding  $\mathbf{P}_{\text{AS}}$  and substituting  $\boldsymbol{\Gamma} = \mathbf{AS} \boldsymbol{\Sigma} \mathbf{S}^H \mathbf{A}^H + \sigma \mathbf{I}_L$ , we get

$$\begin{aligned} \mathbf{P}_{\text{AS}} \boldsymbol{\Gamma} & = \mathbf{AS} (\mathbf{S}^H \mathbf{A}^H \mathbf{AS})^{-1} \mathbf{S}^H \mathbf{A}^H (\mathbf{AS} \boldsymbol{\Sigma} \mathbf{S}^H \mathbf{A}^H + \sigma \mathbf{I}_L) \\ & = \mathbf{AS} (\mathbf{S}^H \mathbf{A}^H \mathbf{AS})^{-1} (\mathbf{S}^H \mathbf{A}^H \mathbf{AS}) \boldsymbol{\Sigma} \mathbf{S}^H \mathbf{A}^H + \sigma \mathbf{AS} (\mathbf{S}^H \mathbf{A}^H \mathbf{AS})^{-1} \mathbf{S}^H \mathbf{A}^H \\ & = \mathbf{AS} \boldsymbol{\Sigma} \mathbf{S}^H \mathbf{A}^H + \sigma \mathbf{AS} (\mathbf{S}^H \mathbf{A}^H \mathbf{AS})^{-1} \mathbf{S}^H \mathbf{A}^H \\ & = \boldsymbol{\Gamma} - \sigma \mathbf{I}_L + \sigma \mathbf{P}_{\text{AS}} \end{aligned} \quad (\text{B.2})$$

Substituting (B.2) into (B.1), we get

$$\begin{aligned} \sigma^{-1} \text{Tr} \left\{ \mathbf{P}_{\text{AS}}^\perp \mathbf{R} \right\} & \approx \sigma^{-1} \text{Tr} \left\{ \boldsymbol{\Gamma} - \boldsymbol{\Gamma} + \sigma \mathbf{I}_L - \sigma \mathbf{P}_{\text{AS}} \right\} \\ & = \text{Tr} \left\{ \mathbf{P}_{\text{AS}}^\perp \right\} = L - P. \end{aligned} \quad (\text{B.3})$$

where the last equality is due to the fact that the eigenvalues of a projection matrix are either ones or zeros and  $\text{Tr} \left\{ \mathbf{P}_{\text{AS}}^\perp \right\} = \text{rank} \left( \mathbf{P}_{\text{AS}}^\perp \right) = L - P$ .

## Appendix C. MLE of the signal information matrix

We represent (20) and (36) in a general form, and determine a general closed form expression of MLE of  $\mathbf{S}$ , which maximizes

$$-\left[ \ln |\mathbf{S}^H \mathbf{A}^H \mathbf{RAS}| - \ln |\mathbf{S}^H \mathbf{A}^H \mathbf{AS}| \right], \quad (\text{C.1})$$

where  $\mathbf{R}$  is a sample covariance matrix of the hypothesis under consideration. We use the following Lemma [32] to find  $\mathbf{S}$ , that maximizes (C.1)

$$\text{Tr} \left\{ \mathbf{C}^{-1} \mathbf{D} \right\} \geq n |\mathbf{C}^{-1} \mathbf{D}|^{\frac{1}{n}} \quad (\text{C.2})$$

where  $\mathbf{C}$  is a positive definite matrix of size  $n$ , and  $\mathbf{D}$  is any arbitrary positive definite matrix of size  $n$ . Taking the logarithm on both sides and rearranging the terms we get

$$\ln |\mathbf{C}| - \ln |\mathbf{D}| \geq n \ln n - n \ln \text{Tr} \left\{ \mathbf{C}^{-1} \mathbf{D} \right\}. \quad (\text{C.3})$$

The inequality in (C.3) does not change by taking logarithm on both sides because logarithm is a monotonically increasing function. Rewriting (C.1) using (C.3), we get

$$\begin{aligned} \ln |\mathbf{S}^H \mathbf{A}^H \mathbf{RAS}| - \ln |\mathbf{S}^H \mathbf{A}^H \mathbf{AS}| \\ \geq P \ln P - P \ln \text{Tr} \left\{ (\mathbf{S}^H \mathbf{A}^H \mathbf{RAS})^{-1} \mathbf{S}^H \mathbf{A}^H \mathbf{AS} \right\} \end{aligned} \quad (\text{C.4})$$

where  $\text{rank} (\mathbf{S}^H \mathbf{A}^H \mathbf{RAS}) = \text{rank} (\mathbf{S}^H \mathbf{A}^H \mathbf{AS}) = \text{rank} (\mathbf{S}) = P$ . The matrix  $\mathbf{A}^H \mathbf{RA}$  is positive definite (for  $D > L$ ) and is a Hermitian matrix; hence, it can be factorized orthogonally. Let  $\mathbf{P} \boldsymbol{\Omega}^{1/2} \boldsymbol{\Omega}^{1/2} \mathbf{P}^H$  be the orthogonal factorization of  $\mathbf{A}^H \mathbf{RA}$ , such that  $\mathbf{P} \mathbf{P}^H = \mathbf{I}_M$  and  $\boldsymbol{\Omega} = \text{diag} \{ \omega_1, \dots, \omega_M \}$  with  $\omega_1 \geq \dots \geq \omega_M$ . In the left hand side of (C.4), the columns of  $\mathbf{S}$  are multiplied with the  $P$  dominant eigenvectors of  $\mathbf{A}^H \mathbf{RA}$ . In order to determine  $\mathbf{S}$  for which equality is achieved in (C.4), we rewrite  $\text{Tr} \left\{ (\mathbf{S}^H \mathbf{A}^H \mathbf{RAS})^{-1} \mathbf{S}^H \mathbf{A}^H \mathbf{AS} \right\}$  as follows:

$$\text{Tr} \left\{ (\mathbf{S}^H \mathbf{A}^H \mathbf{RAS})^{-1} \mathbf{S}^H \mathbf{A}^H \mathbf{AS} \right\} = k \text{Tr} \left\{ \mathbf{S} (\mathbf{S}^H \mathbf{P} \boldsymbol{\Omega}^{1/2} \boldsymbol{\Omega}^{1/2} \mathbf{P}^H \mathbf{S})^{-1} \mathbf{S}^H \right\}, \quad (\text{C.5})$$

where we have used the identity  $\mathbf{A}^H \mathbf{A} = k \mathbf{I}_M$ . Let us define  $\mathbf{K} \triangleq \boldsymbol{\Omega}^{1/2} \mathbf{P}^H \mathbf{S}$ . Rewriting (C.5), we get

$$\begin{aligned} \text{Tr} \left\{ (\mathbf{S}^H \mathbf{A}^H \mathbf{RAS})^{-1} \mathbf{S}^H \mathbf{A}^H \mathbf{AS} \right\} & = k \text{Tr} \left\{ \boldsymbol{\Omega}^{-1/2} \mathbf{K} (\mathbf{K}^H \mathbf{K})^{-1} \mathbf{K}^H \boldsymbol{\Omega}^{-1/2} \right\} \\ & = k \text{Tr} \left\{ \boldsymbol{\Omega}^{-1} \mathbf{H} \right\} \end{aligned} \quad (\text{C.6})$$

where we have used the orthonormal property  $\mathbf{P} \mathbf{P}^H = \mathbf{I}_M$ , and defined  $\mathbf{H} \triangleq \mathbf{K} (\mathbf{K}^H \mathbf{K})^{-1} \mathbf{K}^H$ . Here,  $\mathbf{H}$  takes the form of a projection matrix, such that  $\text{rank} (\mathbf{H}) = \text{rank} (\mathbf{K}) = \text{rank} (\mathbf{S}) = P < M$ . Then, (C.6) can be expressed as

$$k \text{Tr} \left\{ \boldsymbol{\Omega}^{-1} \mathbf{H} \right\} = k \sum_{i=1}^M \frac{h_{i,i}}{\omega_i} \geq k \sum_{i=1}^P \frac{h_{i,i}}{\omega_i}, \quad (\text{C.7})$$

where  $h_{i,i}$  and  $\omega_i$  represent the diagonal entries of the matrix  $\mathbf{H}$  and  $\boldsymbol{\Omega}$ , respectively. The eigenvalues of  $\mathbf{H}$  are either ones or zeros because  $\mathbf{H}$  takes the form of a projection matrix,  $0 \leq h_{i,i} \leq 1$ , and  $\text{Tr} \{ \mathbf{H} \} = \text{rank} (\mathbf{H}) = P$ . We want the dominant eigenvalues to appear on the right hand side of (C.4). Hence, in order to achieve equality in (C.4),  $\mathbf{H}$  takes the form

$$\mathbf{H} = \begin{bmatrix} \mathbf{I}_P & \mathbf{0}_{P, M-P} \\ \mathbf{0}_{M-P, P} & \mathbf{0}_{M-P, M-P} \end{bmatrix} = \mathbf{K} (\mathbf{K}^H \mathbf{K})^{-1} \mathbf{K}^H. \quad (\text{C.8})$$

where  $\mathbf{0}_{N_1, N_2}$  represents a zero matrix of size  $N_1 \times N_2$ . We partition  $\mathbf{P}$  such that,  $\mathbf{P} \triangleq \left[ \mathbf{P}_1 \quad \mathbf{P}_2 \right]$ , where  $\mathbf{P}_1 \in \mathbb{C}^{M \times P}$  and  $\mathbf{P}_2 \in \mathbb{C}^{M \times (M-P)}$  are orthogonal column vectors that satisfy  $\mathbf{P}_1^H \mathbf{P}_1 = \mathbf{I}_P$ ,  $\mathbf{P}_2^H \mathbf{P}_2 = \mathbf{I}_{M-P}$ ,  $\mathbf{P}_1^H \mathbf{P}_2 = \mathbf{0}_{P, M-P}$ , and  $\mathbf{P}_2^H \mathbf{P}_1 = \mathbf{0}_{M-P, P}$ . Similarly, we partition  $\boldsymbol{\Omega}^{1/2} = \text{diag} \{ \boldsymbol{\Omega}_1^{1/2}, \boldsymbol{\Omega}_2^{1/2} \}$ , where  $\boldsymbol{\Omega}_1^{1/2} \in \mathbb{C}^{P \times P}$  and  $\boldsymbol{\Omega}_2^{1/2} \in \mathbb{C}^{(M-P) \times (M-P)}$ . Then  $\mathbf{K}$  can be expressed as

$$\begin{aligned} \mathbf{K} & = \boldsymbol{\Omega}^{1/2} \mathbf{P}^H \mathbf{S} = \begin{bmatrix} \boldsymbol{\Omega}_1^{1/2} & \mathbf{0} \\ \mathbf{0} & \boldsymbol{\Omega}_2^{1/2} \end{bmatrix} \begin{bmatrix} \mathbf{P}_1^H \mathbf{S} \\ \mathbf{P}_2^H \mathbf{S} \end{bmatrix} \\ & = \begin{bmatrix} \boldsymbol{\Omega}_1^{1/2} \mathbf{P}_1^H \mathbf{S} \\ \boldsymbol{\Omega}_2^{1/2} \mathbf{P}_2^H \mathbf{S} \end{bmatrix} \triangleq \begin{bmatrix} \mathbf{K}_1 \\ \mathbf{K}_2 \end{bmatrix}. \end{aligned} \quad (\text{C.9})$$

Since  $\mathbf{K}^H \mathbf{K}$  is full rank, it is invertible and hence not equal to zero matrix. In order to satisfy (C.8),

$$\mathbf{K}_2 = \boldsymbol{\Omega}_2^{1/2} \mathbf{P}_2^H \mathbf{S} = \mathbf{0}. \quad (\text{C.10})$$

The column vectors of  $\mathbf{P}_1$  and  $\mathbf{P}_2$  are orthogonal. Hence, (C.10) is satisfied when  $\mathbf{S} = \mathbf{P}_1\mathbf{T}$ , where  $\mathbf{P}_1$  represents the eigenvectors corresponding to the  $P$  largest eigenvalues of  $\mathbf{A}^H\mathbf{R}\mathbf{A}$ , and  $\mathbf{T}$  is some unitary transform matrix that satisfies  $\mathbf{T}^H\mathbf{T} = \mathbf{T}\mathbf{T}^H = \mathbf{I}_P$ . Then  $\mathbf{K}$  can be expressed as follows:

$$\mathbf{K} = \begin{bmatrix} \mathbf{K}_1 \\ \mathbf{K}_2 \end{bmatrix} = \begin{bmatrix} \boldsymbol{\Omega}_1^{1/2}\mathbf{T} \\ \mathbf{0} \end{bmatrix}. \quad (\text{C.11})$$

Substituting  $\mathbf{K}$  in (C.8), we get

$$\begin{aligned} \mathbf{H} &= \begin{bmatrix} \mathbf{I}_P & \mathbf{0}_{P,M-P} \\ \mathbf{0}_{M-P,P} & \mathbf{0}_{M-P,M-P} \end{bmatrix} \\ &= \begin{bmatrix} \boldsymbol{\Omega}_1^{1/2}\mathbf{T}(\mathbf{T}^H\boldsymbol{\Omega}_1\mathbf{T})^{-1}\mathbf{T}^H\boldsymbol{\Omega}_1^{1/2} & \mathbf{0}_{P,M-P} \\ \mathbf{0}_{M-P,P} & \mathbf{0}_{M-P,M-P} \end{bmatrix}. \end{aligned} \quad (\text{C.12})$$

The first block matrix in (C.12) is equal to  $\mathbf{I}_P$  when  $\mathbf{T} = \mathbf{I}_P$ . Hence,  $\mathbf{S} = \mathbf{P}_1$ , which represents the eigenvector corresponding to the  $P$  largest eigenvalues of  $\mathbf{A}^H\mathbf{R}\mathbf{A}$ . On substituting  $\mathbf{S} = \mathbf{P}_1$  in (C.4), the equality condition is true when all the  $P$  dominant eigenvalues of  $\mathbf{A}^H\mathbf{R}\mathbf{A}$  are equal.

#### Appendix D. MLE of the target scattering matrix coefficients

In this section, we derive the MLE of  $\boldsymbol{\mu}$  in (31). The only term that depends on  $\boldsymbol{\mu}$  in (31) is  $\ln|\mathbf{S}^H\mathbf{A}^H\mathbf{R}_1\mathbf{A}\mathbf{S}|$ . Since, the logarithm of a determinant is a log-concave function, a maximum value exists. In order to find the maximum value, we take the first order derivative of  $\ln|\mathbf{S}^H\mathbf{A}^H\mathbf{R}_1\mathbf{A}\mathbf{S}|$  and equate it to zero. For simplicity in notation while calculating the derivative, we denote  $\mathbf{Q} = (\mathbf{S}^H\mathbf{A}^H\mathbf{R}_1\mathbf{A}\mathbf{S})^{-1}$  and  $\mathbf{M} = \mathbf{A}\mathbf{S}$ . Using the derivative rule  $\frac{d}{d\boldsymbol{\mu}} \ln|\mathbf{C}| = \text{Tr}\{\mathbf{C}^{-1}\frac{d}{d\boldsymbol{\mu}}\mathbf{C}\}$ , we get

$$\frac{\partial}{\partial \boldsymbol{\mu}} \ln|\mathbf{M}^H\mathbf{R}_1\mathbf{M}| = \text{Tr}\left\{\mathbf{Q}\frac{\partial}{\partial \boldsymbol{\mu}}\mathbf{M}^H\mathbf{R}_1\mathbf{M}\right\} = \text{Tr}\left\{\mathbf{M}\mathbf{Q}\mathbf{M}^H\frac{\partial}{\partial \boldsymbol{\mu}}\mathbf{R}_1\right\}. \quad (\text{D.1})$$

Let  $\mathbf{W} = \mathbf{M}\mathbf{Q}\mathbf{M}^H$ , and by expanding  $\mathbf{R}_1$ , we get

$$\mathbf{R}_1 = \mathbf{R}_0 - \bar{\mathbf{y}}\boldsymbol{\mu}^H\mathbf{N}^H - \mathbf{N}\boldsymbol{\mu}\bar{\mathbf{y}}^H + \mathbf{N}\boldsymbol{\mu}\boldsymbol{\mu}^H\mathbf{N}^H.$$

where  $\mathbf{N} = \mathbf{B}\mathbf{S}$ . Since  $\boldsymbol{\mu}$  is a complex vector, we take the partial derivative with respect to  $\Re\{\boldsymbol{\mu}\}$  and  $\Im\{\boldsymbol{\mu}\}$ , where  $\Re$  and  $\Im$  represent the real and imaginary parts of the complex vector, respectively. Therefore, the derivative can be expressed as

$$\text{Tr}\left\{\mathbf{W}\frac{\partial}{\partial \boldsymbol{\mu}}\mathbf{R}_1\right\} = \text{Tr}\left\{\mathbf{W}\frac{\partial \mathbf{R}_1}{\partial \Re\{\boldsymbol{\mu}\}}\right\} - j\text{Tr}\left\{\mathbf{W}\frac{\partial \mathbf{R}_1}{\partial \Im\{\boldsymbol{\mu}\}}\right\}. \quad (\text{D.2})$$

We use the following derivative rules [33] to further simplify the (D.2):

$$\frac{\partial \text{Tr}\{\boldsymbol{\mu}\}}{\partial \Re\{\boldsymbol{\mu}\}} = 1 \quad j\frac{\partial \text{Tr}\{\boldsymbol{\mu}\}}{\partial \Im\{\boldsymbol{\mu}\}} = -1 \quad (\text{D.3})$$

$$\frac{\partial \text{Tr}\{\mathbf{G}\boldsymbol{\mu}\}}{\partial \Re\{\boldsymbol{\mu}\}} = \mathbf{G}^T \quad j\frac{\partial \text{Tr}\{\mathbf{G}\boldsymbol{\mu}\}}{\partial \Im\{\boldsymbol{\mu}\}} = -\mathbf{G}^T \quad (\text{D.4})$$

$$\frac{\partial \text{Tr}\{\mathbf{G}\boldsymbol{\mu}^H\}}{\partial \Re\{\boldsymbol{\mu}\}} = \mathbf{G} \quad j\frac{\partial \text{Tr}\{\mathbf{G}\boldsymbol{\mu}^H\}}{\partial \Im\{\boldsymbol{\mu}\}} = \mathbf{G} \quad (\text{D.5})$$

for some arbitrary matrix  $\mathbf{G}$ . Expanding the first term in Eq. (D.2) gives the following:

$$\begin{aligned} &\text{Tr}\left\{\mathbf{W}\frac{\partial \mathbf{R}_1}{\partial \Re\{\boldsymbol{\mu}\}}\right\} \\ &= \text{Tr}\left\{\mathbf{W}\frac{\partial}{\partial \Re\{\boldsymbol{\mu}\}}(\mathbf{R}_0 - \bar{\mathbf{y}}\boldsymbol{\mu}^H\mathbf{N}^H - \mathbf{N}\boldsymbol{\mu}\bar{\mathbf{y}}^H + \mathbf{N}\boldsymbol{\mu}\boldsymbol{\mu}^H\mathbf{N}^H)\right\}. \end{aligned} \quad (\text{D.6})$$

The first term in (D.6) does not depend on  $\boldsymbol{\mu}$ , whereas each of the remaining three terms can be further simplified using the derivative rules expressed in (D.3)–(D.5) as follows:

$$\text{Tr}\left\{-\frac{\mathbf{N}^H\mathbf{W}\bar{\mathbf{y}}\partial \boldsymbol{\mu}^H}{\partial \Re\{\boldsymbol{\mu}\}}\right\} = -\mathbf{N}^H\mathbf{W}\bar{\mathbf{y}},$$

$$\text{Tr}\left\{-\frac{\bar{\mathbf{y}}^H\mathbf{W}\mathbf{N}\partial \boldsymbol{\mu}}{\partial \Re\{\boldsymbol{\mu}\}}\right\} = -(\bar{\mathbf{y}}^H\mathbf{W}\mathbf{N})^T,$$

$$\text{Tr}\left\{\frac{\mathbf{N}^H\mathbf{W}\mathbf{N}\partial(\boldsymbol{\mu}\boldsymbol{\mu}^H)}{\partial \Re\{\boldsymbol{\mu}\}}\right\} = (\boldsymbol{\mu}^H\mathbf{N}^H\mathbf{W}\mathbf{N})^T + (\mathbf{N}^H\mathbf{W}\mathbf{N}\boldsymbol{\mu}).$$

Combining all the terms, we get

$$\begin{aligned} \text{Tr}\left\{\mathbf{W}\frac{\partial}{\partial \Re\{\boldsymbol{\mu}\}}\mathbf{R}_1\right\} &= -(\mathbf{N}^H\mathbf{W}\bar{\mathbf{y}}) - (\bar{\mathbf{y}}^H\mathbf{W}\mathbf{N})^T \\ &\quad + (\boldsymbol{\mu}^H\mathbf{N}^H\mathbf{W}\mathbf{N})^T + (\mathbf{N}^H\mathbf{W}\mathbf{N}\boldsymbol{\mu}). \end{aligned} \quad (\text{D.7})$$

In a similar way, expanding the second term in (D.2) gives

$$\begin{aligned} &j\text{Tr}\left\{\mathbf{W}\frac{\partial}{\partial \Im\{\boldsymbol{\mu}\}}\mathbf{R}_1\right\} \\ &= j\text{Tr}\left\{\mathbf{W}\frac{\partial}{\partial \Im\{\boldsymbol{\mu}\}}(\mathbf{R}_0 - \bar{\mathbf{y}}\boldsymbol{\mu}^H\mathbf{N}^H - \mathbf{N}\boldsymbol{\mu}\bar{\mathbf{y}}^H + \mathbf{N}\boldsymbol{\mu}\boldsymbol{\mu}^H\mathbf{N}^H)\right\}. \end{aligned}$$

We ignore the first term because it does not depend on  $\boldsymbol{\mu}$ . Simplifying each of the remaining three terms further using the derivative rules in (D.3)–(D.5) we get,

$$j\text{Tr}\left\{-\frac{\mathbf{N}^H\mathbf{W}\bar{\mathbf{y}}\partial \boldsymbol{\mu}^H}{\partial \Im\{\boldsymbol{\mu}\}}\right\} = -\mathbf{N}^H\mathbf{W}\bar{\mathbf{y}},$$

$$j\text{Tr}\left\{-\frac{\bar{\mathbf{y}}^H\mathbf{W}\mathbf{N}\partial \boldsymbol{\mu}}{\partial \Im\{\boldsymbol{\mu}\}}\right\} = (\bar{\mathbf{y}}^H\mathbf{W}\mathbf{N})^T,$$

$$j\text{Tr}\left\{\frac{\mathbf{N}^H\mathbf{W}\mathbf{N}\partial(\boldsymbol{\mu}\boldsymbol{\mu}^H)}{\partial \Im\{\boldsymbol{\mu}\}}\right\} = (\mathbf{N}^H\mathbf{W}\mathbf{N}\boldsymbol{\mu}) - (\boldsymbol{\mu}^H\mathbf{N}^H\mathbf{W}\mathbf{N})^T.$$

Combining all the terms, we get

$$\begin{aligned} j\text{Tr}\left\{\mathbf{W}\frac{\partial}{\partial \Im\{\boldsymbol{\mu}\}}\mathbf{R}_1\right\} &= -(\mathbf{N}^H\mathbf{W}\bar{\mathbf{y}}) + (\bar{\mathbf{y}}^H\mathbf{W}\mathbf{N})^T \\ &\quad - (\boldsymbol{\mu}^H\mathbf{N}^H\mathbf{W}\mathbf{N})^T + (\mathbf{N}^H\mathbf{W}\mathbf{N}\boldsymbol{\mu}). \end{aligned} \quad (\text{D.8})$$

Substituting (D.7) and (D.8) into (D.2), we get

$$\text{Tr}\left\{\mathbf{W}\frac{\partial}{\partial \boldsymbol{\mu}}\mathbf{R}_1\right\} = 2(\boldsymbol{\mu}^H\mathbf{N}^H\mathbf{W}\mathbf{N})^T - 2(\bar{\mathbf{y}}^H\mathbf{W}\mathbf{N})^T. \quad (\text{D.9})$$

Equating (D.9) to zero, we get

$$(\bar{\mathbf{y}} - \mathbf{N}\boldsymbol{\mu})^H\mathbf{W}\mathbf{N} = \mathbf{0}.$$

The matrix  $\mathbf{W}\mathbf{N}$  cannot be a zero matrix. So, it follows that the MLE of  $\boldsymbol{\mu}$ , denoted as  $\hat{\boldsymbol{\mu}}$ , is given as

$$\hat{\boldsymbol{\mu}} = \mathbf{N}^\dagger \bar{\mathbf{y}} = (\mathbf{B}\mathbf{S})^\dagger \bar{\mathbf{y}}. \quad (\text{D.10})$$

#### References

- [1] H. Griffiths, C. Baker, Passive coherent location radar systems. part 1: performance prediction, IEE Proc. Radar Son. Nav. 152 (3) (2005) 153–159.
- [2] C. Baker, H. Griffiths, I. Papoutsis, Passive coherent location radar systems. part 2: waveform properties, IEE Proc. Radar Son. Nav. 152 (3) (2005) 160–168.
- [3] M.A. Ringer, G.J. Frazer, Waveform analysis of transmissions of opportunity for passive radar, Signal Processing and Its Applications, 1999. ISSPA '99. Proceedings of the Fifth International Symposium on, Brisbane, Qld., vol. 2, 1999, pp. 511–514.
- [4] A.G. Westra, Radar Versus Stealth: Passive Radar and the Future of US Military Power, Technical Report, DTIC Document, 2009.
- [5] A. Nehorai, E. Paldi, Vector-sensor array processing for electromagnetic source localization, IEEE Trans. Signal Process. 42 (2) (1994) 376–398.
- [6] R. Saini, M. Cherniakov, DTV signal ambiguity function analysis for radar application, IEE Proc. Radar Son. Nav. 152 (3) (2005) 133–142.

- [7] J. Palmer, H. Harms, S. Searle, L. Davis, DVB-T passive radar signal processing, *IEEE Trans. Signal Process.* 61 (8) (2013) 2116–2126.
- [8] C. Berger, B. Demissie, J. Heckenbach, P. Willett, S. Zhou, Signal processing for passive radar using OFDM waveforms, *IEEE J. Sel. Top Signal Process.* 4 (1) (2010) 226–238.
- [9] S. Gogineni, M. Rangaswamy, B. Rigling, A. Nehorai, Ambiguity function analysis for UMTS-based passive multistatic radar, *IEEE Trans. Signal Process.* 62 (11) (2014) 2945–2957.
- [10] F. Colone, D.W. O'Hagan, P. Lombardo, C.J. Baker, A multistage processing algorithm for disturbance removal and target detection in passive bistatic radar, *IEEE Trans. Aerosp Electron Syst* 45 (2) (2009) 698–722.
- [11] X. Zhang, H. Li, J. Liu, B. Himed, Joint delay and doppler estimation for passive sensing with direct-path interference, *IEEE Trans. Signal Process.* 64 (3) (2016) 630–640.
- [12] D. Hack, L. Patton, B. Himed, M. Saville, Centralized passive MIMO radar detection without direct-path reference signals, *IEEE Trans. Signal Process.* 62 (11) (2014) 3013–3023.
- [13] K.S. Bialkowski, I.V.L. Clarkson, S.D. Howard, Generalized canonical correlation for passive multistatic radar detection, 2011 *IEEE Statistical Signal Processing Workshop (SSP)*, Nice, 2011, pp. 417–420.
- [14] J. Liu, H. Li, B. Himed, Two target detection algorithms for passive multistatic radar, *IEEE Trans. Signal Process.* 62 (22) (2014) 5930–5939.
- [15] L. Wang, B. Yazici, Passive imaging of moving targets using sparse distributed apertures, *SIAM J. Imaging Sci.* 5 (3) (2012) 769–808.
- [16] National Research Council, *Weather Radar Technology Beyond NEXRAD*, The National Academies Press, Washington, DC, 2002.
- [17] P.L. Smith, On the sensitivity of weather radars, *J. Atmos. Oceanic Technol.* 3 (4) (1986) 704–713.
- [18] V.N. Bringi, V. Chandrasekar, *Polarimetric doppler weather radar*, Cambridge University Press, 2001.
- [19] R. Compton, The tripole antenna: an adaptive array with full polarization flexibility, *IEEE Trans. Antennas Propag.* 29 (6) (1981) 944–952.
- [20] W.-M. Boerner, M. El-Arini, C.-Y. Chan, P. Mastoris, Polarization dependence in electromagnetic inverse problems, *IEEE Trans. Antennas Propag.* 29 (2) (1981) 262–271.
- [21] H. Li, Z. Wang, J. Liu, B. Himed, Moving target detection in distributed MIMO radar on moving platforms, *IEEE J. Sel. Top Signal Process.* 9 (8) (2015) 1524–1535.
- [22] M. Hurtado, A. Nehorai, Polarimetric detection of targets in heavy inhomogeneous clutter, *IEEE Trans. Signal Process.* 56 (4) (2008) 1349–1361.
- [23] C.F. Loan, The ubiquitous kronecker product, *J. Comput Appl Math* 123 (12) (2000) 85–100. *Numerical Analysis 2000. Vol. III: Linear Algebra*.
- [24] R.J. Doviak, V. Bringi, A. Ryzhkov, A. Zahrai, D. Zrnić, Considerations for polarimetric upgrades to operational WSR-88D radars, *J. Atmos. Oceanic Technol.* 17 (3) (2000) 257–278.
- [25] B. Hochwald, A. Nehorai, Polarimetric modeling and parameter estimation with applications to remote sensing, *IEEE Trans. Signal Process.* 43 (8) (1995) 1923–1935.
- [26] A.W. Van der Vaart, *Asymptotic Statistics*, vol. 3, Cambridge University Press, 2000.
- [27] R. Vershynin, How close is the sample covariance matrix to the actual covariance matrix? *J. Theor. Probab.* 25 (3) (2012) 655–686.
- [28] D.A. Harville, *Matrix Algebra from a Statistician's Perspective*, vol. 1, Springer, 1997.
- [29] T.W. Anderson, *An Introduction to Multivariate Statistical Analysis*, vol. 2, Wiley New York, 1958.
- [30] S.M. Kay, *Fundamentals of statistical signal processing*, Vol. II: Detection Theory, Signal Processing, Prentice Hall, Upper Saddle River, NJ, 1998.
- [31] P. Stoica, A. Nehorai, On the concentrated stochastic likelihood function in array signal processing, *Circ. Syst. Signal Process.* 14 (5) (1995) 669–674.
- [32] J. Burg, D. Luenberger, D. Wenger, Estimation of structured covariance matrices, *Proc. IEEE* 70 (9) (1982) 963–974.
- [33] A. Hjørungnes, D. Gesbert, Complex-valued matrix differentiation: techniques and key results, *IEEE Trans. Signal Process.* 55 (6) (2007) 2740–2746.